People's Democratic Republic of Algeria
Ministry Of Higher Education And Scientific Reseach

University of KASDI Merbah - Ouargla
Faculty of Mathematics and Material Science
Department of Physics

Professional Master's Thesis

Domain: Physics

Specialty: Medical Physics

Presented by :

LARGOT Imane

Theme :

ECG Simulation Using a Hybrid Gaussian-Dipole Model

12/06/ 2025

in front of the jury members

Dr. AYAT Zahia	University of Ouargla	President
Dr. MOKADEM Zakaria	University of Ouargla	Jury
Pr. BENTOUILA Omar	University of Ouargla	Supervisor

Academic year : 2024/2025

ملخص

طوّرنا في هذا البحث نموذجًا هجينًا يجمع بين الدوال الغاوسية والتمثيل ثنائي القطب لمحاكاة تخطيط كهربية القلب. أظهر النموذج دقة عالية في محاكاة القطب الثاني، وأداءً مقبولاً للأقطاب الاثني عشر، مع قدرة فعّالة على محاكاة الأمراض القلبية مثل نقص التروية وتسارع النظم البطيني. يتميز النموذج بالكفاءة الحاسوبية والمرونة وقابلية التطبيق في مجالات متعددة تشمل التحقق من صحة خوارزميات التشخيص، والتعليم الطبي، وأبحاث أمراض القلب. غير أن النموذج يواجه تحديات تتمثل في انخفاض دقة تقدير معاملات الأقطاب الاثني عشر ومحدودية في تمثيل التباين بين النبضات القلبية. يساهم هذا النموذج في تطوير خوارزميات التشخيص الطبي، وأنظمة المحاكاة التعليمية، وطب القلب الحاسوبي، مما يفتح آفاقًا لتحسين رعاية المرضى ونتائج العلاج.

كلمات مفتاحية: تخطيط كهربية القلب، محاكاة، غاوسي، نموذج ثنائي القطب للقلب

Abstract

In this work, we developed a hybrid Gaussian-Dipole model for ECG simulation, combining Gaussian functions with a dipole-based representation of the heart's electrical activity. The model achieved high fidelity for Lead II and reasonable performance across 12-leads, effectively simulating pathologies like ischemia and ventricular tachycardia. The model's strengths include efficiency, flexibility, and applicability to algorithm validation, medical education, and cardiac research. However, limitations include less accurate 12-lead parameter estimation and limited capture of beat-to-beat variability. This work advances diagnostic algorithm development, medical training simulation systems, and computational cardiology, offering potential improvements in patient care and clinical outcomes.

Key words: *ECG, Simulation, Gaussian, Heart-Dipole Model*

Acknowledgements

All praise is due to Allah, who granted me faith, courage, and patience to complete this work.

I extend my heartfelt gratitude to my supervisor, Professor Omar BENTOUILA , for his trust in me, his constant presence, dedicated efforts, guidance, humility, advice, and constructive feedback, which significantly contributed to the success of this work.

I express my sincere appreciation to the esteemed committee members, Dr. Zahia Ayat and Dr. Mokaddem Zakaria, for discussing my thesis.

I renew my thanks to my supervisor, in his capacity as the director of the LENREZA laboratory, for providing us with all the necessary conditions to complete this work.

I offer my heartfelt thanks to everyone who contributed, directly or indirectly, to the development of this work, and to all those who helped me improve it.

As I near the culmination of this academic journey, I would like to thank all my esteemed professors who taught me throughout my university journey.

May Allahs peace and blessings be upon our noble Prophet, his family, and all his companions.

الإهداء

الحمد لله أولاً وآخراً، الحمد لله حمداً كثيراً طيباً مباركاً فيه.
الحمد لله العلي القدير الذي وفقني لإنجاز هذا العمل.

أهدي هذا البحث إلى:

قرة عيني وروح فؤادي.. سندي بعد الله **أمي**

عزوتي.. قوتي وسندي بعد الله **أبي**

أعز ما أملك إخوتي **وليد** و**عبد النور** وجميع إخوتي

إيمان

Contents

List of Figures

List of Tables

General introduction

The electrocardiogram (ECG) stands as one of the most fundamental diagnostic tools in modern cardiology, offering a non-invasive window into the heart's electrical activity [1]. Since its inception over a century ago with the pioneering work of Waller [2] and subsequent development by Willem Einthoven in 1924 [3], who was awarded the Nobel Prize for his contributions, the ECG has proven invaluable for detecting cardiac arrhythmias, conduction abnormalities, ischemic heart disease, myocardial infarction, and various electrolyte disorders [4, 5]. The ECG captures potential differences on the body surface caused by depolarization and repolarization of the heart muscle, thus providing valuable information about the electrical state and function of the heart. However, the complexity of interpreting ECG signals and understanding the intricate relationship between cardiac electrophysiology and surface potentials presents ongoing challenges for both clinicians and researchers [6].

The advent of computational modeling has revolutionized our approach to understanding and simulating cardiac electrical activity [7, 8]. ECG simulation models serve multiple critical functions in cardiovascular medicine and research by providing controlled environments for investigating the fundamental mechanisms linking cellular electrophysiology to the characteristic waveforms observed on surface recordings [9]. These models are essential for developing and validating automated ECG analysis algorithms, particularly for rare or complex arrhythmias that may be underrepresented in clinical databases [10]. Educational applications represent another significant domain where ECG simulators prove their worth, allowing medical students and healthcare professionals to practice ECG interpretation on diverse signal patterns in a safe, interactive environment [11].

Medical physics plays a vital role in the development and refinement of ECG technology. Medical physicists engage in the design and optimization of recording instruments, the modeling of electrical signaling in biological tissues (the forward problem), and the intricate processing and analysis of ECG signals for precise diagnostic information extraction (the inverse problem) [12, 13]. These tasks encompass noise filtering, characteristic wave detection (QRS complex), analysis of heart rate variability (HRV), and the construction of

mathematical models to interpret ECG signals accurately.

While real ECG data is readily available in medical databases like PhysioNet [14, 15], the need to simulate synthetic ECG signals is surging due to multiple factors. Firstly, acquiring sufficiently large datasets with all pathological conditions to effectively train and test diagnostic algorithmsespecially AI-based onesproves challenging [16]. Secondly, synthetic signals enable complete control of all signal parameters including heart rate, waveform morphology, noise level, and specific abnormalities, making them ideal for systematic testing and performance evaluation of signal processing algorithms and automated diagnostic systems [17]. Thirdly, simulation serves as an invaluable pedagogical tool for students in medicine, medical physics, and engineering to understand ECG dynamics and the influence of various physiological and pathological states [18]. Finally, simulation can be utilized to create test data for evaluating the safety and robustness of cardiac monitoring devices.

This thesis addresses these challenges by developing a novel hybrid Gaussian-Dipole model for ECG simulation, designed to balance physiological realism with computational efficiency. The model combines Gaussian functions to represent the temporal morphology of ECG waveforms with a dipole-based approach to capture the spatial projection of cardiac electrical activity across multiple leads. By leveraging real ECG data from the MIT-BIH Arrhythmia Database, the model is parameterized to simulate both Lead II and 12-lead ECGs, including pathological conditions such as ischemia and atrial fibrillation. The primary objectives of this work are to review existing ECG simulation methods, formulate and implement the hybrid model, evaluate its performance against real data using quantitative metrics, and discuss its potential applications and limitations.

In the preparation of this thesis, artificial intelligence tools were utilized to enhance the quality and presentation of the research work. Specifically, AI-assisted tools were employed for text refinement and rephrasing to improve clarity and coherence, formatting consistency to ensure professional presentation standards, and debugging programming code to identify and correct computational errors in the simulation algorithms. These tools served as supportive instruments to augment the research process while maintaining the scientific integrity and originality of the work.

The thesis is structured as follows: Chapter 1 provides the theoretical foundations of ECG signals, covering cardiac anatomy, electrophysiology, and the 12-lead system. Chapter 2 explores physical and mathematical models for cardiac electrical activity, laying the groundwork for the hybrid approach. Chapter 3 details the methodology, including data processing, model implementation, and evaluation as well as the results for Lead II and 12-lead

simulations and discusses the model's strengths, limitations, and future directions.

Through this work, we aim to contribute a versatile tool for medical physics, supporting advancements in cardiac diagnostics, algorithm development, and education in the face of the growing global cardiovascular disease burden.

Chapter 1

Theoretical Foundations of ECG Signals

1.1 Introduction

The electrocardiogram (ECG) is a fundamental non-invasive diagnostic tool that records the electrical activity of the heart over time. It plays a critical role in the detection and monitoring of various cardiac pathologies, including arrhythmias, ischemic events such as myocardial infarction, and conduction system disorders. While modern ECG systems have been significantly enhanced by digital signal processing, machine learning, and wearable technologies, the accurate interpretation and development of such systems still rely heavily on a deep understanding of the physiological mechanisms underlying ECG waveforms.

This chapter provides a comprehensive overview of the theoretical foundations necessary to interpret ECG signals from both a biological and physical perspective. It begins with a brief historical and technological context before delving into cardiac anatomy and the specialized structures responsible for the initiation and propagation of the cardiac impulse. A detailed explanation of cellular electrophysiologyparticularly action potentialis followed by a description of how these microscopic events translate into macroscopic ECG waveforms. This foundation serves as an essential prerequisite for the mathematical and computational modeling approaches explored in subsequent chapters.

1.2 Historical and Technological Background

The origins of electrocardiography go back to the late 19th century, with pioneering work by scientists such as Galvani in 1791, Matteucci in 1842, and Kölliker Müller in 1855, who investigated electrical currents in muscle contractions [19]. The first recordings of the electrical activity of the heart on the body surface were made by Augustus Desiré Waller in 1887 using the capillary electrometer developed by Lippmann [2]. However, it was Willem Einthoven who laid the true foundation for clinical electrocardiography. In 1903, he introduced the string galvanometer, a groundbreaking device that allowed precise measurement of the electrical potentials of the heart and led to the definition of the PQRST complex [3]. Einthovens pioneering work earned him the Nobel Prize in Physiology or Medicine in 1924 and marked the birth of modern cardiology.

Following Einthovens breakthrough, researchers like Thomas Lewis and Francis Wilson further advanced the understanding of cardiac electrophysiology, particularly in the realm of arrhythmias and interpretation of the ECG [20]. During the past century, ECG technology has undergone a significant evolution, from early analog devices to sophisticated digital systems equipped with microprocessors, advanced filtering algorithms, wireless transmission capabilities and artificial intelligence for automated rhythm analysis [21, 22]. The emergence of portable and wearable ECG monitors has expanded thier application beyond traditional clinical settings, especially for long-term cardiac surveillance [23, 24, 25].

Despite these technological advancements, the biophysical principles governing ECG signal generation remain unchanged. A solid understanding of these principles continues to be essential for clinicians and researchers aiming to develop novel diagnostic tools or refine existing methodologies in the ever-evolving field of electrocardiography.

1.3 Cardiac Anatomy and Electrical Conduction

1.3.1 Cardiac Chambers

The heart consists of four chambers two atria and two ventricles each playing a distinct and essential role in the circulatory function of the cardiovascular system.

- **Right Atrium**: The right atrium receives deoxygenated blood from the systemic circulation via the superior and inferior venae cavae, as well as the coronary sinus [26]. Its interior is divided into three anatomical regions: the *sinus venarum* (smooth posterior wall), the anterior portion lined with parallel muscular ridges called *pectinate muscles*, and the *atrial*

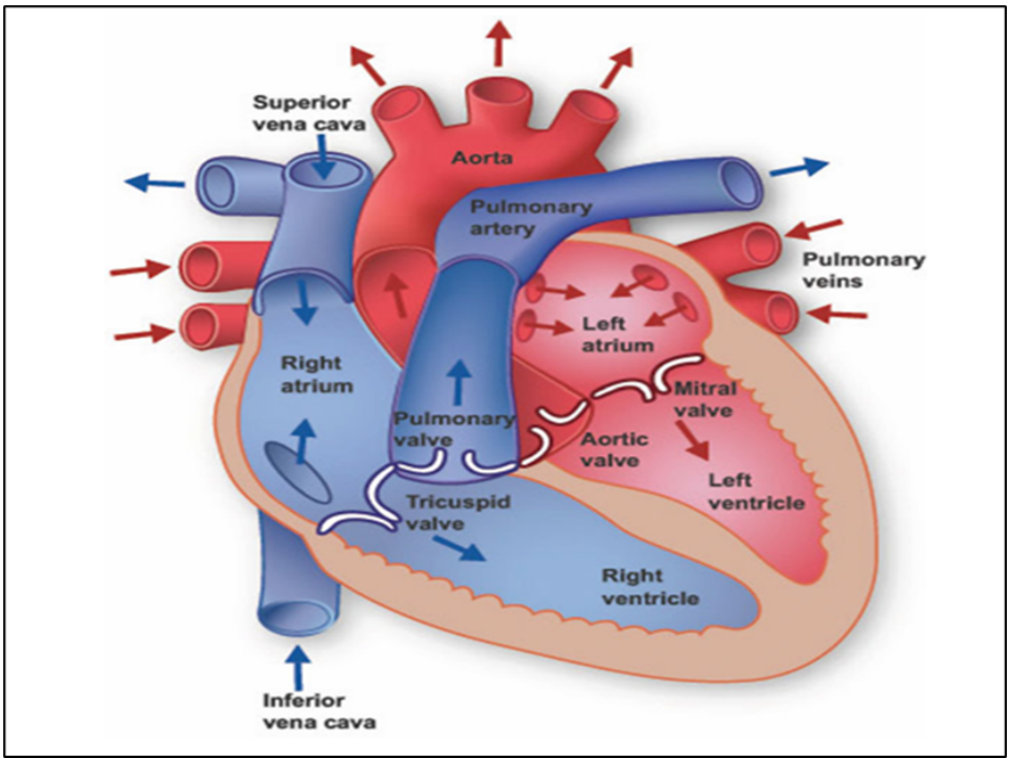

Figure 1.1: Diagram of the human heart with labeled chambers and valves [7].

septum. It contains several key structures, including the **sinoatrial (SA) node**, which acts as the hearts primary pacemaker, the **atrioventricular (AV) node**, and the **fossa ovalis**, a remnant of the fetal foramen ovale [27].

- **Left Atrium**: Positioned posterior to the right atrium and superior to the left ventricle, the left atrium receives oxygenated blood from the lungs through the pulmonary veins. Like the right atrium, it has a smooth-walled main chamber and a pectinate atrial appendage. It plays a crucial role in delivering oxygen-rich blood to the left ventricle during diastole [28].

- **Right Ventricle**: The right ventricle pumps deoxygenated blood from the right atrium into the pulmonary trunk, which carries it to the lungs for oxygenation. It forms most of the anterior surface of the heart and contains prominent muscular structures known as *trabeculae carneae*. The outflow tract of the right ventricle, called the *conus arteriosus* or *infundibulum*, is smooth-walled and separates the left and right ventricular outflow tracts [29].

- **Left Ventricle**: The left ventricle is responsible for pumping oxygenated blood into the systemic circulation via the aorta. Due to the high pressure required for systemic circulation, it has the thickest myocardial wall among all four chambers. Its internal surface is marked by fine trabeculae carneae and strong papillary muscles. The left ventricle forms most of the left lateral surface of the heart, and its contraction is critical for maintaining adequate blood

flow to body tissues [1].

Enclosed within the pericardial sac, the hearts muscular architecture ensures synchronized contraction and relaxation cycles, enabling efficient pumping and optimal circulatory performance.

1.3.2 Cardiac Valves

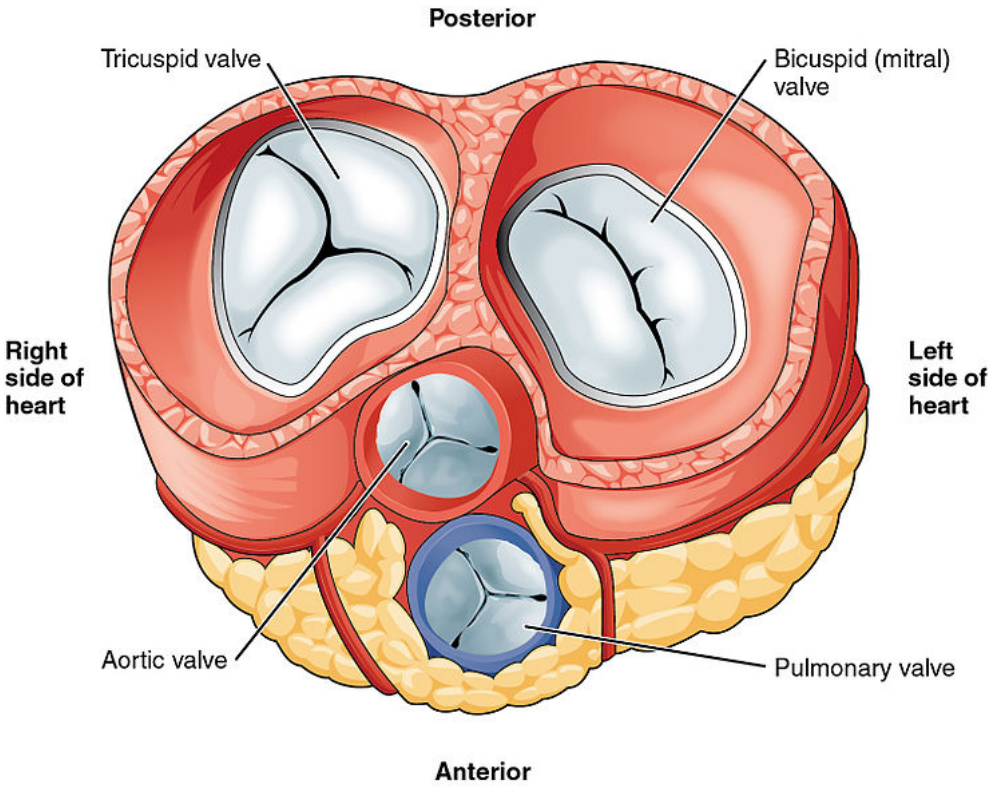

Figure 1.2: Heart valves [30].

The unidirectional flow of blood through the heart is ensured by four major cardiac valves, each playing a crucial role in maintaining efficient circulation. These valves prevent retrograde blood flow during the cardiac cycle and are supported by specialized structures such as chordae tendineae and papillary muscles to ensure proper function and prevent prolapse during systolic contraction [26].

- **Tricuspid Valve**: Located between the right atrium and right ventricle, this valve consists of an annulus, three leaflets (anterior, posterior, and septal), papillary muscles, and chordae tendineae. It prevents backflow of blood into the right atrium during ventricular systole and partially separates the inflow and outflow tracts of the right ventricle [31].

- **Pulmonary Semilunar Valve**: Positioned at the exit of the right ventricle, this valve guards the orifice leading into the pulmonary artery. It comprises three symmetric cusps anterior, left, and right that resemble parachutes in shape. During diastole, these cusps meet centrally within the lumen to block retrograde blood flow from the pulmonary trunk back into the right ventricle [32].

- **Mitral (Bicuspid) Valve**: Situated between the left atrium and left ventricle, the mitral valve has two leaflets anterior and posterior along with chordae tendineae and two papillary muscles. The fibrous annulus supports most of the valve structure, while the medial portion receives support from adjacent aortic structures. This valve ensures one-way flow of oxygenated blood from the left atrium into the left ventricle during diastole [31].

- **Aortic Semilunar Valve**: Found at the junction of the left ventricle and the ascending aorta, this valve consists of three semilunar-shaped cusps attached to a fibrous annulus. During systole, it allows ejection of oxygenated blood into the systemic circulation, and during diastole, it closes tightly to prevent regurgitation. The sinotubular ridge, a circular anatomical landmark on the aortic wall, contributes to the structural integrity of this valve complex [1].

These valves work in coordination with the myocardial contraction cycle to maintain optimal hemodynamic efficiency throughout the cardiovascular system.

1.3.3 Pericardium

The pericardium is a protective, double-layered membranous sac that surrounds the heart and plays a critical role in maintaining its anatomical position and reducing mechanical stress during cardiac activity [26]. It consists of three main layers:

- **Fibrous Pericardium**: This is the outermost layer, composed of dense connective tissue. It forms a loose-fitting sac around the heart, extending over the diaphragm and attaching to the bases of the great vessels. The fibrous pericardium anchors the heart within the mediastinum and prevents excessive distension of the cardiac chambers [27].

- **Parietal Layer of the Serous Pericardium**: This serous membrane lines the inner surface of the fibrous pericardium. It forms the boundary of the pericardial cavity and works in conjunction with the visceral layer to facilitate smooth cardiac motion[33].

- **Visceral Layer of the Serous Pericardium (Epicardium)**: This layer directly covers the surface of the myocardium and is considered part of the heart wall. It secretes lubricating fluid into the pericardial cavity and contributes to the structural integrity of the heart [28].

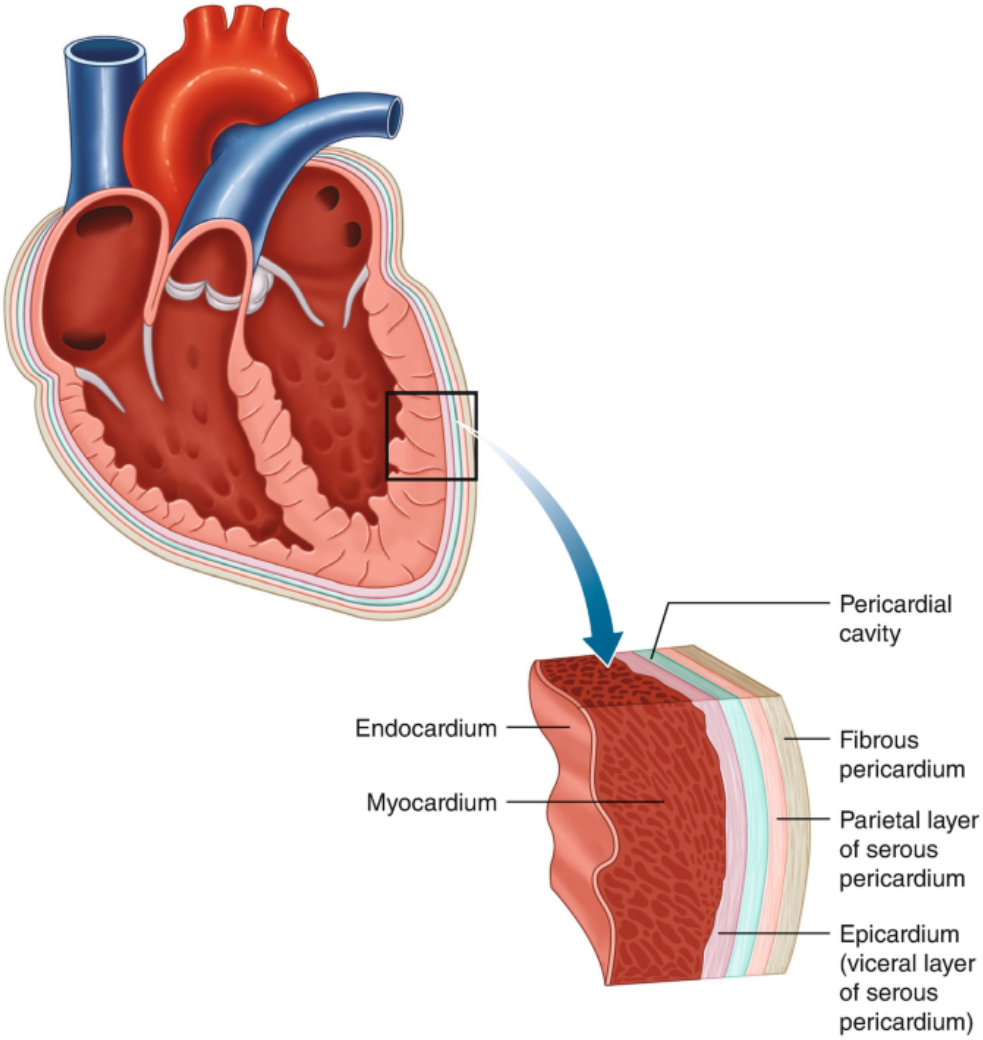

Figure 1.3: Pericardium [33].

Between the parietal and visceral layers lies the pericardial cavity, which contains a small volume of serous fluid. This fluid acts as a lubricant, minimizing friction between the heart and surrounding structures during contraction and relaxation cycles.

1.4 Cardiac Conduction System

The cardiac conduction system is a network of specialized myocardial cells responsible for the generation and coordinated propagation of electrical impulses throughout the heart. This system ensures synchronized and rhythmic contractions necessary for effective cardiac function [1, 28].

- **Sinoatrial (SA) Node**: Positioned in the upper posterior wall of the right atrium

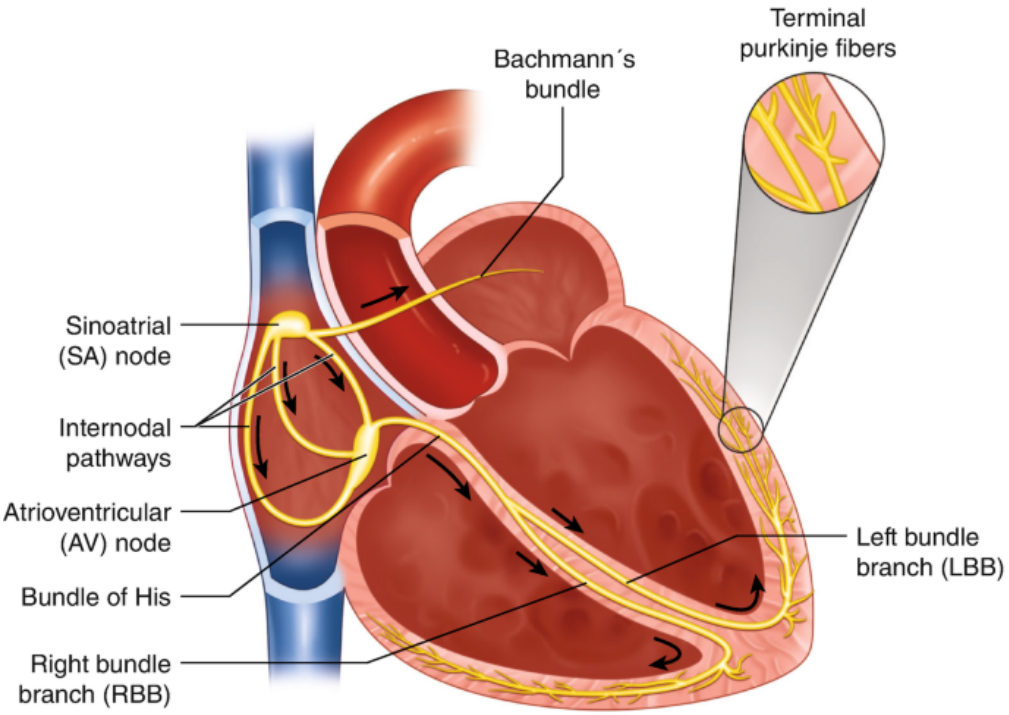

Figure 1.4: Cardiac Conduction System.

near the entrance of the superior vena cava, the SA node acts as the hearts primary pacemaker. Its cells exhibit spontaneous depolarization, initiating the cardiac rhythm at a rate of approximately 60100 beats per minute under normal conditions. The nodes activity is modulated by autonomic innervation, local blood flow, and various chemical factors [34, 27].

- **Intra-atrial and Internodal Pathways**: These pathways facilitate the rapid spread of the impulse across both atria. Three major tracts have been identified the anterior (via Bachmann's bundle to the left atrium), middle (Wenckebach pathway), and posterior (Thorel pathway) which ensure efficient signal transmission to the AV node[35].

- **Atrioventricular (AV) Node**: Located within Kochs triangle in the right atrium, the AV node serves as a critical relay point between the atria and ventricles. It introduces a physiological delay in impulse transmission (reflected as the PR interval on the ECG), allowing sufficient time for ventricular filling before contraction. The node contains fast and slow conduction pathways; the fast pathway conducts quickly but has a longer refractory period, while the slow pathway recovers more rapidly, offering protection against excessive ventricular rates during tachyarrhythmias.

- **Bundle of His**: This structure represents the sole electrical connection between the atria and ventricles. It originates from the AV node and extends into the interventricular septum, where it bifurcates into the left and right bundle branches.

- **Left and Right Bundle Branches & Purkinje Fibers**: The right bundle branch transmits the impulse to the right ventricle, while the left bundle branch divides into anterior and posterior fascicles to supply different regions of the left ventricle. These signals are then distributed through the Purkinje fiber network, which ensures rapid and nearly simultaneous activation of ventricular myocardium, resulting in synchronized contraction [36]. These fibers are anatomically variable and extend into trabeculae such as the moderator band, playing a key role in ventricular excitation.

Disruptions at any level of the conduction system may lead to arrhythmias or conduction blocks, often detectable through characteristic changes in ECG morphology and timing[37]. Understanding this system is essential for diagnosing and managing cardiac rhythm disorders.

1.5 Electrophysiological Basis of ECG Waves

The electrocardiogram (ECG) reflects the summation of electrical activity generated by cardiac myocytes during the cardiac cycle. This bioelectrical activity originates from depolarization and repolarization processes in myocardial and pacemaker cells, which are governed by specific ion currents across the cell membrane.

1.5.1 Phases of the Cardiac Action Potential

Each heartbeat begins with an action potential in pacemaker or working myocardial cells, consisting of five distinct phases (Figure 1.5):

1. **Phase 0 (Rapid Depolarization)**: Voltage-gated sodium (Na^+) channels open at a threshold potential (70 mV), leading to a rapid influx of Na^+ and a sharp rise in membrane potential.

2. **Phase 1 (Initial Repolarization)**: Brief opening of transient outward potassium (K^+) channels causes partial repolarization.

3. **Phase 2 (Plateau Phase)**: A balance between inward calcium (Ca^{2+}) current and sustained K^+ efflux maintains the depolarized state, prolonging contraction duration.

4. **Phase 3 (Repolarization)**: Increased K^+ conductance and closure of Ca^{2+} channels restore the resting membrane potential (90 mV).

5. **Phase 4 (Resting/Spontaneous Depolarization)**: In pacemaker cells (e.g., SA node), a slow inward current (I_h) gradually depolarizes the membrane toward threshold,

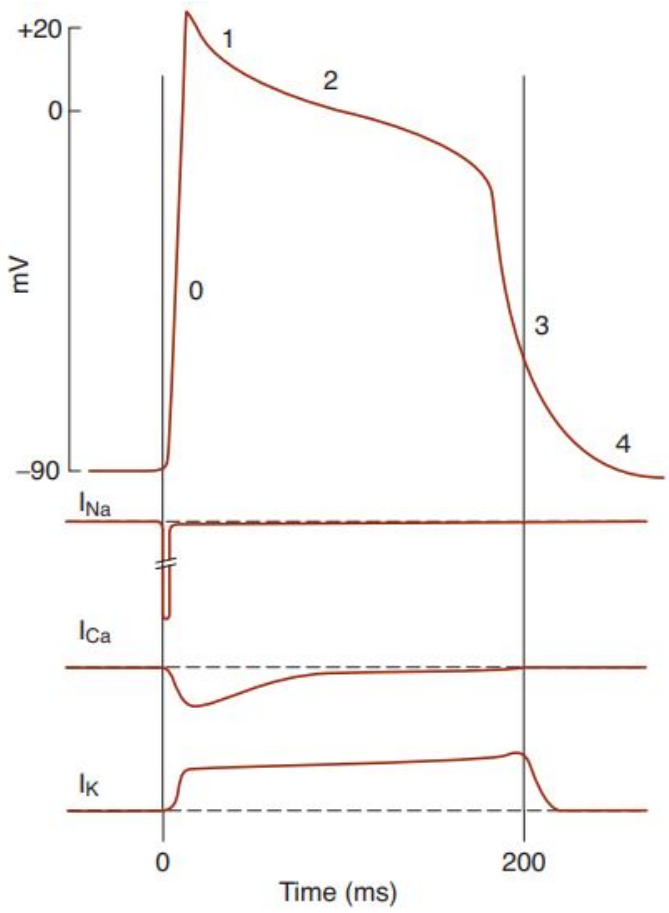

Figure 1.5: Cardiac Action Potential: Phases and Ionic Currents[38].

enabling automaticity. The intrinsic firing rate of the SA node is typically 60100 beats per minute.

These phases are mediated by specific ion channels and transporters, and their coordinated activation determines the shape and duration of the action potential, which directly influences ECG morphology.

1.5.2 ECG Waveform Interpretation

The standard ECG waveform represents the cumulative extracellular manifestation of these cellular events across the entire myocardium. Each component correlates with a specific stage of cardiac electrical activity:

As shown in Figure 1.6, the cardiac impulse starts at the sinoatrial (SA) node, initiating atrial contraction (P wave). It then travels through the atrioventricular (AV) node, where a brief delay ensures complete ventricular filling before ventricular activation (QRS

Table 1.1: ECG components and corresponding cardiac events.

Segment	**Description**
P Wave	Atrial depolarization initiated by the SA node
PR Interval	Time from onset of atrial to ventricular depolarization; includes AV nodal delay
QRS Complex	Ventricular depolarization; large amplitude due to massive ventricular mass
ST Segment	Period between ventricular depolarization and repolarization
T Wave	Ventricular repolarization
QT Interval	Total duration of ventricular electrical activity (from Q onset to T end)

complex) via the Bundle of His, bundle branches, and Purkinje fibers. Finally, ventricular repolarization generates the T wave, completing the cardiac cycle.

This coordinated propagation occurs via gap junctions low-resistance connections that allow the myocardium to function as a functional syncytium, ensuring rapid and synchronized contraction [27].

Abnormalities in ECG waveform morphology or timing often reflect underlying pathologies such as arrhythmias, ischemia, or conduction disorders, making the ECG a cornerstone of clinical cardiology.

1.6 Lead Systems and Cardiac Axis

The 12-lead electrocardiogram (ECG) represents a fundamental diagnostic modality in clinical cardiology and medical physics, enabling the non-invasive assessment of the hearts electrical activity. This technique relies on the spatial recording of cardiac bioelectric potentials through a standardized configuration of limb and precordial leads. These leads provide orthogonal projections of the cardiac dipole vector in both the frontal and horizontal planes, thereby facilitating the detection and localization of various pathological conditions, including arrhythmias, conduction abnormalities, myocardial ischemia, and structural alterations. The recorded signals originate from transmembrane ionic currents associated with myocardial depolarization and repolarization, which propagate through conductive body tissues and are detected as potential differences on the body surface. This section explores the electrophysi-

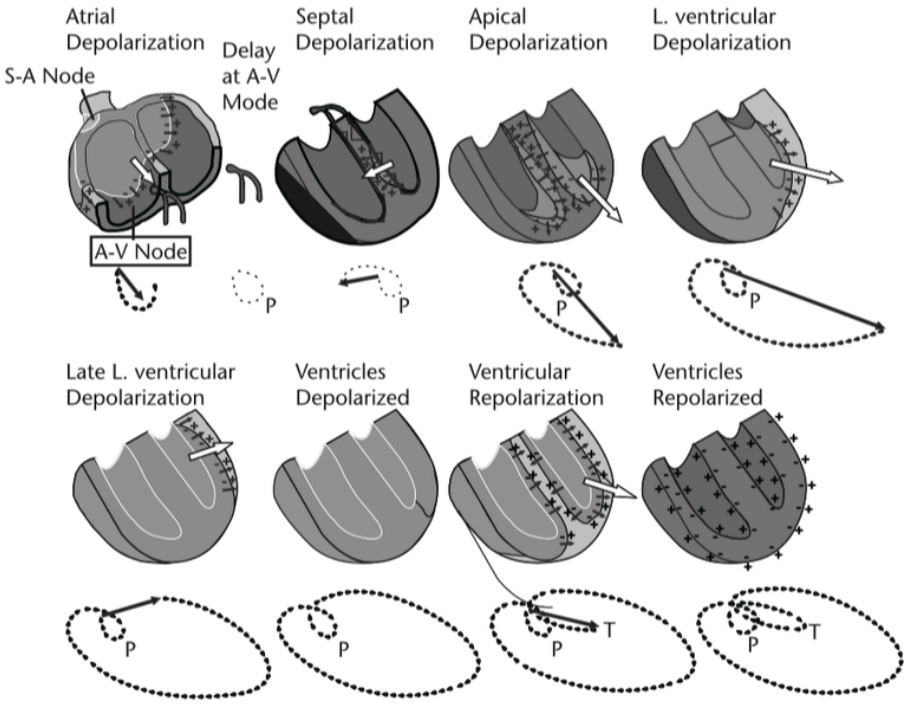

Figure 1.6: Trajectory of a normal cardiac vector[39].

ological and physical principles underlying ECG signal generation, with particular emphasis on dipole theory, lead system orientation, and mathematical modeling of extracellular potentials, in relation to their application in clinical diagnostics and biomedical research.

1.6.1 12-Lead ECG Configuration

The 12-lead ECG system uses limb and precordial leads to record cardiac electrical activity:

- **Bipolar Limb Leads (I, II, III)**: These form Einthovens triangle in the frontal plane, with electrodes on the right arm (RA), left arm (LA), and left leg (LL):

$$V_I = V_{LA} - V_{RA} \tag{1.1}$$

$$V_{II} = V_{LL} - V_{RA} \tag{1.2}$$

$$V_{III} = V_{LL} - V_{LA} \tag{1.3}$$

  Einthovens law ensures consistency:

$$V_{II} = V_I + V_{III} \tag{1.4}$$

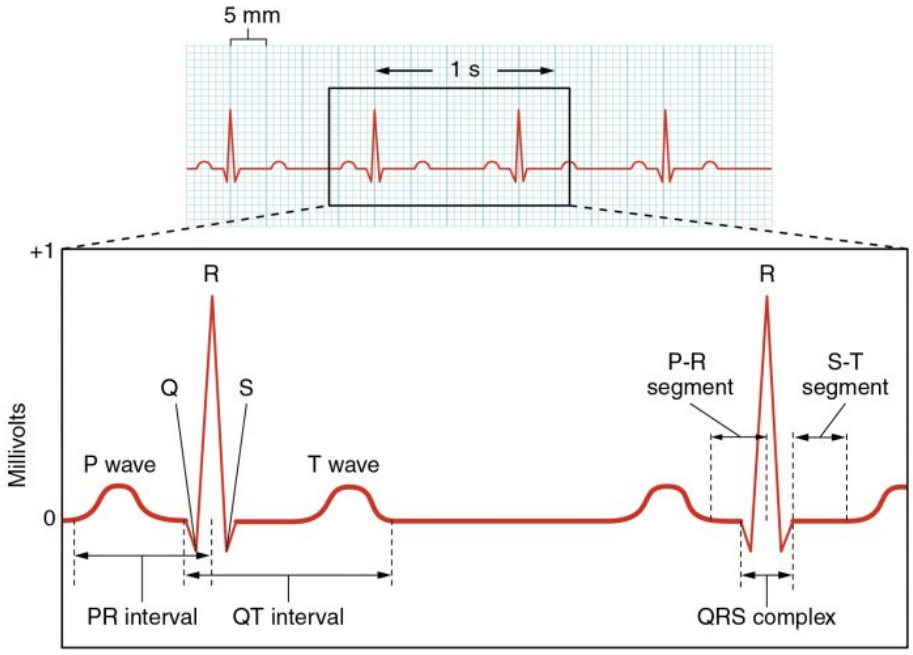

Figure 1.7: The standard ECG waveforms [40].

- **Augmented Unipolar Limb Leads (aVR, aVL, aVF)**: Referenced to Wilsons central terminal:

$$V_W = \frac{V_{RA} + V_{LA} + V_{LL}}{3} \tag{1.5}$$

The augmented leads are:

$$V_{aVR} = \frac{2V_{RA} - V_{LA} - V_{LL}}{3} \tag{1.6}$$

$$V_{aVL} = \frac{2V_{LA} - V_{RA} - V_{LL}}{3} \tag{1.7}$$

$$V_{aVF} = \frac{2V_{LL} - V_{RA} - V_{LA}}{3} \tag{1.8}$$

- **Precordial Leads ($\mathbf{V_1}$$\mathbf{V_6}$)**: Unipolar leads on the chest, referenced to V_W, capture horizontal-plane activity:

$$V_{V_i} = V_{\text{Chest}_i} - V_W \quad \text{for } i = 1 \text{ to } 6 \tag{1.9}$$

These leads enable localization of myocardial injury, hypertrophy, or conduction abnormalities by providing multi-plane views.

1.6.2 Cardiac Vector and Lead Orientation

The hearts electrical activity is modeled as a time-varying cardiac dipole, $\vec{D}(t) = D_x(t)\hat{i} + D_y(t)\hat{j} + D_z(t)\hat{k}$, representing summed myocardial action potentials. The ECG signal is the

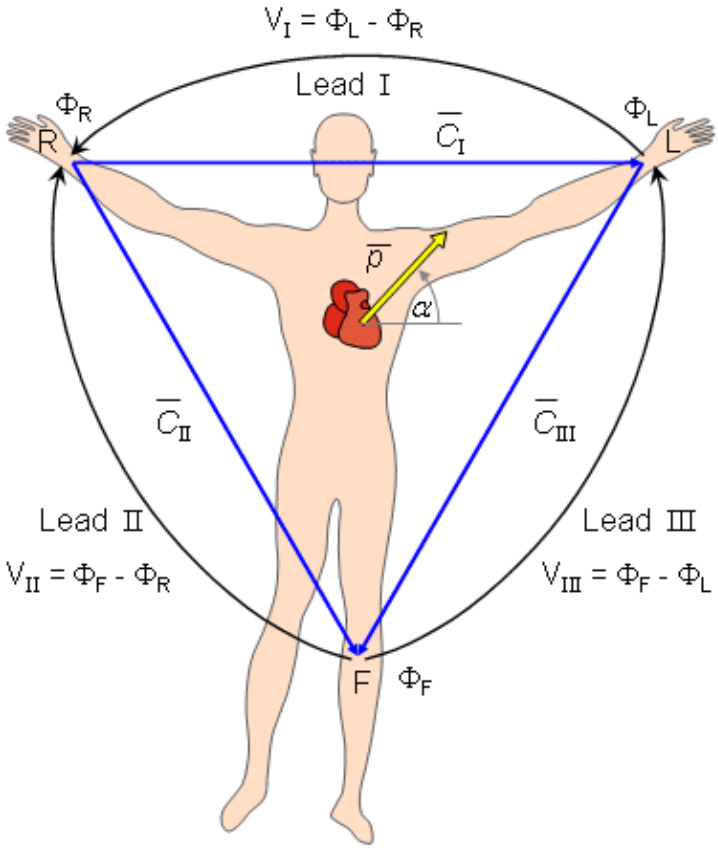

Figure 1.8: Einthoven limb leads and Einthoven triangle

Figure 1.9: Einthovens triangle and hexaxial reference system, showing bipolar (I, II, III) and augmented leads (aVR, aVL, aVF), with precordial lead placements.

projection onto the lead axis:

$$\mathrm{ECG}_{\mathrm{lead}}(t) = \vec{D}(t) \cdot \hat{L} = |\vec{D}(t)| \cos(\theta) \tag{1.10}$$

where $\hat{L}$ is the leads unit vector, and θ is the angle between $\vec{D}(t)$ and $\hat{L}$. The mean electrical axis, derived from Leads I and aVF, ranges from 0° to 90° normally, with deviations indicating pathologies [26].

The extracellular potential is governed by the Poisson equation:

$$\nabla^2 \phi(r,t) = -\frac{\nabla \cdot \vec{J}_s(r,t)}{\sigma} \tag{1.11}$$

where $\vec{J}_s(r,t)$ is the source current density and σ is tissue conductivity.

Figure 1.10: Cardiac dipole $\vec{D}(t)$ projections onto lead vectors, showing deflection types.

1.6.3 Physical Basis of ECG Signal Generation

ECG signals arise from ionic currents during depolarization and repolarization. The resting transmembrane potential ($V_m \approx -80\,\text{mV}$ to $-90\,\text{mV}$) is set by ion gradients, per the Nernst equation:

$$E_{\text{ion}} = \frac{RT}{zF} \ln \left(\frac{[\text{ion}]_{\text{out}}}{[\text{ion}]_{\text{in}}} \right) \tag{1.12}$$

The action potential is modeled by:

$$C_m \frac{dV_m}{dt} = -(I_{Na} + I_K + I_{Ca} + I_{\text{stim}}) \tag{1.13}$$

Extracellular potentials propagate through the body:

$$\phi(\vec{r}, t) = \frac{1}{4\pi\sigma} \int \frac{\vec{J}_s(\vec{r}', t) \cdot (\vec{r} - \vec{r}')}{|\vec{r} - \vec{r}'|^3} \, dV' \tag{1.14}$$

1.6.4 Clinical Applications

The ECG diagnoses:

- **Arrhythmias**: Atrial fibrillation (irregular P waves), ventricular tachycardia (wide QRS).
- **Conduction Disorders**: AV block (prolonged PR), Wolff-Parkinson-White (short PR, delta wave).
- **Myocardial Injury**: ST elevation ($> 1\,\text{mm}$), pathological Q waves.
- **Hypertrophy**: Sokolow-Lyon criteria ($S_{V1} + R_{V5/V6} > 35\,\text{mm}$).
- **Electrolyte Imbalances**: Peaked T waves (hyperkalemia), prolonged QT (hypocalcemia).
- **Pericarditis**: Widespread ST elevation.
- **Pulmonary Embolism**: S1Q3T3 pattern.

1.7 Conclusion

This chapter presented the foundational knowledge required to understand the generation and interpretation of ECG signals. Beginning with the structural organization of the heart and its conduction system, we examined how electrical activation is initiated and propagated through the myocardium. We linked cellular electrophysiology to the formation of ECG waveforms and explained the significance of each component in clinical cardiology. Finally, we reviewed the standard lead configurations and the vector-based approach to interpreting ECG signal morphology.

This theoretical framework provides the essential background for the mathematical and computational models discussed in the following chapter, which will explore the physics and mathematics behind ECG signal simulation and analysis.

Chapter 2

Physical and Mathematical Modeling of Cardiac Electrophysiology

2.1 Introduction

The mathematical modeling of cardiac electrophysiology constitutes a fundamental tool for explaining the electrical functions and basic mechanisms of the heart. This discipline allows to simulate and investigate cardiac electrophysiological phenomena across a spectrum of scales, ranging from individual cardiomyocytes to entire cardiac tissues. These models yield invaluable insights into both normal cardiac physiology and pathological states, thus making considerable contributions to clinical diagnostics and therapeutic interventions.

The electrocardiogram (ECG), a non-invasive diagnostic methode, records the heart's electrical activity via surface electrodes, producing characteristic waveforms[41]. This electrical activity originates within a complex network of specialized cells, beginning at the sinoatrial node and propagating through the atrioventricular conduction system, finally displaying as measurable potentials on the body surface [9]. Accurate simulation of ECG signals is of dominant importance for medical education, the testing of medical devices, the validation of diagnostic algorithms, and computational cardiology [41, 17]. Reaching realistic waveforms requires modelling both the electrophysiology at the cellular level and the macroscopic propagation of electrical fields through cardiac tissue and the torso [42].

This chapter offers a review of ECG simulation models. We will present models that describe cellular action potentials, the propagation of electrical excitation through cardiac tissue, and those for generating ECG waveforms. We will critically evaluate these models based on their physiological accuracy, computational efficiency, and suitability for diverse

applications, including medical training simulators

2.2 Cellular Action Potential Models

The heartbeat begins at the cellular level, where the action potentiala rapid change in a cells electrical potentialdrives cardiac rhythm. Modeling these cellular dynamics is the foundation of cardiac electrophysiology simulations, capturing the interplay of ion flows across the cell membrane.

2.2.1 Hodgkin-Huxley Model

In 1952, Hodgkin and Huxley transformed our understanding of excitable cells with their seminal model of the squid giant axon [43]. This Nobel Prize-winning framework, originally developed for neurons, has become a cornerstone for modeling cardiac cells by describing how voltage-gated ion channels generate action potentials.

2.2.1.1 *Model Description*

The Hodgkin-Huxley model envisions the cell membrane as an electrical circuit, with the lipid bilayer acting as a capacitor and ion channels as variable conductors. It accounts for the flow of sodium (Na^+), potassium (K^+), and leak currents, driven by electrochemical gradients defined by the Nernst potential:

$$V_{\text{ion}} = \frac{RT}{zF} \ln\left(\frac{[\text{ion}]_{\text{out}}}{[\text{ion}]_{\text{in}}}\right) \tag{2.1}$$

Here, $R = 8.314\,\text{J} \cdot \text{K}^{-1} \cdot \text{mol}^{-1}$ is the gas constant, T is the absolute temperature, z is the ions valence, and $F = 96,485\,\text{C} \cdot \text{mol}^{-1}$ is Faradays constant.

The membrane potential V evolves according to:

$$C_m \frac{dV}{dt} = -I_{\text{ion}}(V, m, h, n) + I_{\text{ext}} \tag{2.2}$$

where C_m is the membrane capacitance, I_{ext} is an external stimulus current, and I_{ion} is the total ionic current:

$$I_{\text{ion}} = g_{\text{Na}} m^3 h (V - V_{\text{Na}}) + g_{\text{K}} n^4 (V - V_{\text{K}}) + g_{\text{L}} (V - V_{\text{L}}) \tag{2.3}$$

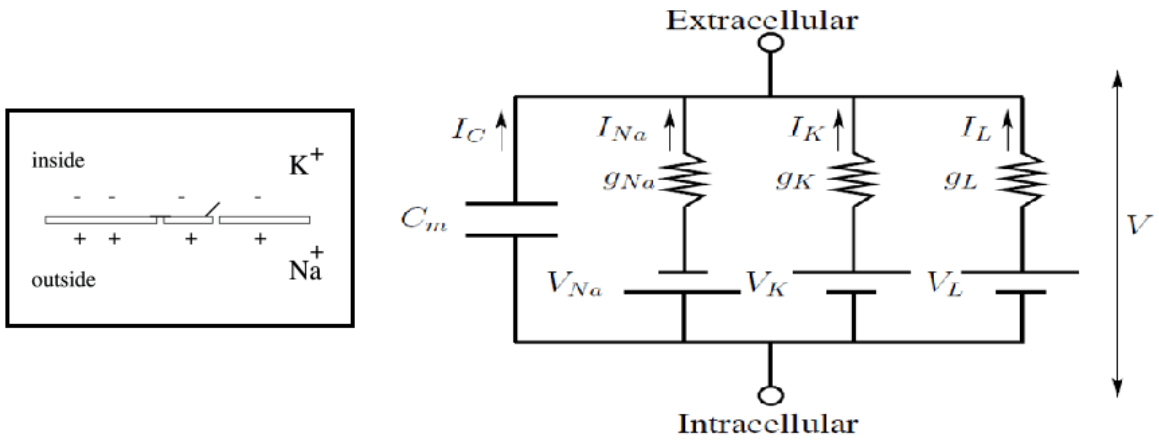

Figure 2.1: Schematic of the Hodgkin-Huxley model, illustrating the membrane as a capacitor with voltage-dependent sodium, potassium, and leak conductances.

The conductances g_{Na}, g_{K}, and g_{L} represent sodium, potassium, and leak channels, respectively, with V_{Na}, V_{K}, and V_{L} as their Nernst potentials. The gating variables m, h, and n describe the probability of channel activation or inactivation, governed by:

$$\frac{dn}{dt} = \alpha_n(V)(1-n) - \beta_n(V)n \tag{2.4}$$

$$\frac{dm}{dt} = \alpha_m(V)(1-m) - \beta_m(V)m \tag{2.5}$$

$$\frac{dh}{dt} = \alpha_h(V)(1-h) - \beta_h(V)h \tag{2.6}$$

The rate constants $\alpha(V)$ and $\beta(V)$ are voltage-dependent, enabling the model to capture the nonlinear dynamics of action potential generation.

2.2.1.2 *Applications*

- Exploring the mechanisms of action potential generation and ion channel dynamics.
- Assessing the impact of pharmacological agents on cardiac cell behavior [41].
- Serving as a foundation for more complex cardiac-specific models.

2.2.1.3 *Limitations*

- Computationally intensive, especially for large-scale simulations involving many cells.

- Requires adaptation for cardiac cells, which have distinct ion channel profiles compared to neurons.
- Challenging to scale to whole-heart models without simplification.

2.2.2 FitzHugh-Nagumo Model

The FitzHugh-Nagumo model, introduced in the early 1960s [44], simplifies the Hodgkin-Huxley framework to capture the essential dynamics of excitability with fewer variables, making it computationally efficient and mathematically tractable.

2.2.2.1 *Model Description*

This model reduces the complex dynamics to two variables: a fast variable v, representing the membrane potential, and a slow variable w, representing recovery processes. The governing equations are:

$$\frac{dv}{dt} = v - \frac{v^3}{3} - w + I \tag{2.7}$$

$$\frac{dw}{dt} = \varepsilon(v + a - bw) \tag{2.8}$$

Here, I is an external stimulus current, $\varepsilon \ll 1$ sets the time scale separation, and a and b adjust the excitation threshold and recovery dynamics. The cubic term in the first equation mimics the rapid depolarization of an action potential, while the slow variable ensures a refractory period.

2.2.2.2 *Applications*

- Modeling wave propagation and spiral waves in cardiac tissue, relevant to arrhythmias.
- Educational tools to demonstrate excitability principles.
- Exploring qualitative dynamics of cardiac excitation.

2.2.2.3 *Advantages*

- Computationally lightweight, enabling large-scale simulations.
- Analytically tractable, supporting phase-plane analysis.
- Captures key features like thresholds and refractory periods.

2.2.2.4 *Limitations*

- Oversimplifies ionic mechanisms, limiting physiological detail.
- Parameters are phenomenological, not directly tied to measurable quantities.
- Less accurate for quantitative predictions compared to biophysical models.

2.3 Propagation of Electrical Excitation in Cardiac Tissue

Once an action potential is initiated, it spreads through the heart, coordinating contraction. Modeling this propagation requires accounting for the tissues complex structure, including its anisotropic electrical properties.

2.3.1 Bidomain Model

The bidomain model is the gold standard for simulating cardiac tissue electrophysiology, offering a detailed representation of electrical activity across intracellular and extracellular domains [45].

2.3.1.1 *Model Description*

This model treats cardiac tissue as two interpenetrating domains: the intracellular space (inside cells) and the extracellular space (outside cells), each with distinct conductivity tensors σ_i and σ_e. The transmembrane potential $V_m = V_i - V_e$ links these domains. The governing equations are:

$$\nabla \cdot (\sigma_i \nabla V_i) = \beta I_m - I_{s,i} \tag{2.9}$$

$$\nabla \cdot (\sigma_e \nabla V_e) = -\beta I_m - I_{s,e} \tag{2.10}$$

where β is the membrane surface-to-volume ratio, $I_{s,i}$ and $I_{s,e}$ are stimulus currents, and I_m is the transmembrane current:

$$I_m = C_m \frac{\partial V_m}{\partial t} + I_{\text{ion}}(V_m, \vec{y}) \tag{2.11}$$

The ionic current I_{ion} is typically defined by a cellular model (e.g., Hodgkin-Huxley), and $\vec{y}$ represents state variables. The bidomain model captures the anisotropic propagation of action potentials, crucial for realistic simulations.

2.3.1.2 *Applications*

- Simulating ECG generation by computing extracellular potentials.
- Studying complex arrhythmias and defibrillation effects.
- Investigating the impact of tissue anisotropy on wave propagation.

2.3.1.3 *Limitations*

- High computational cost due to coupled equations and complex ionic models.
- Requires detailed knowledge of conductivity tensors, which are hard to measure.

2.3.2 Monodomain Model

The monodomain model simplifies the bidomain framework by assuming proportional anisotropy between intracellular and extracellular domains, reducing computational demands.

2.3.2.1 *Model Description*

Assuming $\sigma_e = \lambda \sigma_i$, the bidomain equations reduce to a single reaction-diffusion equation:

$$\beta C_m \frac{\partial V_m}{\partial t} + \beta I_{\text{ion}}(V_m, \vec{y}) = \nabla \cdot (\sigma_{\text{eff}} \nabla V_m) + I_{\text{app}} \tag{2.12}$$

Here, $\sigma_{\text{eff}} = \frac{\lambda}{1+\lambda}\sigma_i$ is the effective conductivity, and I_{app} is an applied stimulus. This model focuses on the transmembrane potential V_m, sacrificing direct computation of extracellular potentials.

2.3.2.2 *Applications*

- Large-scale simulations of action potential propagation.
- Studying wave dynamics and spiral wave formation.

2.3.2.3 *Advantages*

- Lower computational cost than the bidomain model.
- Simpler to implement and solve numerically.

2.3.2.4 *Limitations*

- Cannot directly compute extracellular potentials, limiting ECG applications.
- Assumes proportional anisotropy, which may not hold in pathological conditions.

2.4 Mathematical Models for ECG Waveform Simulation

While biophysical models offer deep mechanistic insights, mathematical models focus on replicating ECG waveforms efficiently, making them ideal for real-time applications and educational tools [41].

2.4.1 Physiological Oscillator Models

The hearts rhythm arises from specialized pacemaker cells. Oscillator-based models capture this rhythmicity by representing key conduction nodes as coupled oscillators.

2.4.1.1 *Van der Pol Oscillators*

The Van der Pol oscillator, originally developed for electrical circuits, models the hearts conduction system using coupled, nonlinear oscillators [46]. The governing equation is:

$$\frac{d^2x}{dt^2} - \mu(1 - x^2)\frac{dx}{dt} + \omega^2 x = 0 \tag{2.13}$$

where μ controls nonlinearity and ω sets the oscillation frequency. Coupled oscillators can represent the sinoatrial node, atrioventricular node, and His-Purkinje system, generating ECG-like signals [**?**].

Advantages: Captures rhythmic behavior and conduction system interactions. **Limitations:** Simplified representation requiring careful parameter tuning.

2.4.2 Morphological Models

Morphological models prioritize replicating the shape of ECG waves (P, QRS, T) using mathematical functions, sacrificing physiological detail for simplicity.

2.4.2.1 *Gaussian Function-Based Models*

Gaussian functions model ECG waves as bell-shaped curves [17]:

$$V(t) = \sum_{i \in \{P,Q,R,S,T\}} A_i \exp\left(-\frac{(t-t_i)^2}{2\sigma_i^2}\right) + V_{\text{baseline}} \tag{2.14}$$

where A_i, t_i, and σ_i define amplitude, timing, and width, respectively. Multi-lead ECGs use lead-specific scaling factors:

$$V_{\text{lead}_j}(t) = \sum_i k_{j,i} A_i \exp\left(-\frac{(t-t_i)^2}{2\sigma_i^2}\right) \tag{2.15}$$

Advantages: Simple, efficient, and intuitive for basic simulators. **Limitations:** Lacks physiological grounding and struggles with complex arrhythmias.

2.4.2.2 *Sinusoidal Waveform Models*

Fourier-based models represent ECGs as sums of sinusoids [**?**]:

$$V(t) = A_0 + \sum_{k=1}^{M} A_k \sin(2\pi f_k t + \phi_k) \tag{2.16}$$

Time-varying parameters $A_k(t)$, $f_k(t)$, and $\phi_k(t)$ incorporate heart rate variability (HRV).

Advantages: Effective for periodic signals and frequency analysis. **Limitations:** Requires many harmonics for sharp features like QRS complexes.

2.4.3 Dynamic Models (ECGD)

Dynamic models generate sequences of heartbeats with realistic variability, crucial for long-term ECG simulations.

2.4.3.1 *McSharry Model*

McSharry et al. proposed a three-dimensional dynamical system to generate ECGs with HRV [17]:

$$\frac{dx}{dt} = \alpha x - \omega y \tag{2.17}$$

$$\frac{dy}{dt} = \alpha y + \omega x \tag{2.18}$$

$$\frac{dz}{dt} = -\sum_{i \in \{P,Q,R,S,T\}} a_i \Delta\theta_i \exp\left(-\frac{\Delta\theta_i^2}{2b_i^2}\right) - (z - z_0) \tag{2.19}$$

The phase angle $\theta = \text{atan2}(y, x)$ drives wave generation, with $z(t)$ as the ECG output. Extensions include HRV effects like respiratory sinus arrhythmia [**?**].

Advantages: Captures waveform morphology and HRV dynamics. **Limitations:** Requires careful parameter tuning and may miss complex pathologies [**?**].

2.4.4 Reaction-Diffusion Models for Waveform

Reaction-diffusion equations, typically used for propagation, can also generate waveforms via their reaction term:

$$\frac{\partial V}{\partial t} = \nabla \cdot (D \nabla V) + f(V, \vec{y}) \tag{2.20}$$

These are valuable for modeling waveform changes due to propagation effects, such as in ischemia.

2.5 Forward Problem of ECG Generation

The forward problem links cardiac electrical activity to body surface potentials, modeling the heart as a source within the torsos volume conductor.

2.5.1 Equivalent Source Models

To simplify the hearts complex activity, equivalent source models are used.

2.5.1.1 *Dipole Models*

A single current dipole $\vec{H}(t)$ approximates the hearts electrical activity, with multi-dipole or multipole expansions for added detail.

2.5.1.2 *Distributed Surface Models*

- **Uniform Double Layer (UDL):** Models the depolarization wavefront as a dipole layer.
- **Equivalent Double Layer (EDL):** Places dipoles on epicardial/endocardial surfaces.
- **Epicardial/Endocardial Potential (EP) Models:** Uses surface potentials as boundary conditions.

2.5.1.3 *Transmembrane Potential (TMP) Models*

TMP models use the myocardial V_m distribution, often from bidomain simulations, to compute surface potentials, offering a direct link to cellular dynamics.

Volume Conductor Model and Solution Methods

The torso is modeled as a heterogeneous conductor, governed by Laplaces or Poissons equation. The Boundary Element Method (BEM) discretizes only interfaces between regions, reducing computational cost compared to Finite Element or Finite Difference methods.

2.6 Physical Models: Linking Cellular Activity to Surface Potentials

Physical models bridge cellular events to ECG signals, providing insights into how microscopic activity translates to clinical measurements

2.6.1 Heart Vector Model (Dipole Model)

The heart vector model simplifies the hearts activity as a single dipole $\vec{H}(t)$, projected onto lead vectors $\vec{L}$ to compute ECG voltages [47]:

$$V_{\text{lead}}(t) = \vec{H}(t) \cdot \vec{L} \tag{2.21}$$

Lead vectors for the 12-lead ECG are derived from geometric assumptions like Einthovens triangle [48]. This model supports multi-lead ECG synthesis [49].

Advantages: Intuitive, efficient, and suitable for multi-lead ECGs. **Limitations:** Oversimplifies distributed sources and struggles with localized pathologies.

2.7 Deep Learning-Based Models

Deep learning offers innovative solutions for generating realistic ECGs, particularly for data-intensive applications.

2.7.1 Generative Adversarial Networks (GANs)

GANs use a generator and discriminator to produce synthetic ECGs, with conditional GANs enabling targeted generation for specific conditions.

Applications: Data augmentation, pathology simulation, and anonymization.

Advantages: Highly realistic outputs and flexibility.

Limitations: Training instability and data requirements.

Chapter 3

ECG Simulation using Hybrid Gaussian-Dipole Model

3.1 Introduction

Current approaches to ECG simulation span a broad spectrum, from simple mathematical functions to sophisticated biophysical models [41]. At one end, basic models employ combinations of elementary waveformssuch as Gaussians, sine waves, or polynomialsto approximate the characteristic P-QRS-T complex. While computationally efficient, these approaches often lack physiological realism and may struggle to accurately represent the variability seen in clinical practice, particularly under pathological conditions.

At the opposite extreme, detailed biophysical models simulate electrical activity at the cellular or tissue level, incorporating anatomical heart geometry and solving complex partial differential equations [45, 50]. These models offer exceptional fidelity but require substantial computational resources and extensive parameterization, limiting their practical application in real-time scenarios or large-scale studies.

The hybrid Gaussian-Dipole model presented in this chapter represents a promising middle ground between these approaches. By combining the mathematical simplicity of Gaussian functions with the physiological insight of dipole modeling [51, 5], this framework aims to balance computational efficiency with biological plausibility. The model leverages Gaussian functions to represent individual ECG components (P, QRS, and T waves) while employing a dipole vector to capture the heart's overall electrical orientation. This dipole is then projected onto standard lead axes to generate realistic multi-lead ECG signals.

This work details the development and application of this hybrid model for simulating

both standard Lead II ECG signals and comprehensive 12-lead recordings. We explore the mathematical foundations, parameter estimation methodologies using real ECG data from the MIT-BIH Arrhythmia Database [52], and the practical implementation in Python. The model's performance is evaluated through comparison with actual recordings, and its versatility is demonstrated through simulation of various pathological conditions.

3.2 Theoretical Background and Model Formulation

3.2.1 Gaussian Representation of ECG Components

The choice of Gaussian functions for modeling ECG waveforms stems from their natural ability to approximate the smooth, bell-shaped characteristics commonly observed in physiological signals [17]. A Gaussian function provides a mathematically tractable representation while maintaining biological plausibility for cardiac electrical events.

The fundamental Gaussian function is defined as:

$$G(t, A, \mu, \sigma) = A \cdot \exp\left(-\frac{(t-\mu)^2}{2\sigma^2}\right) \tag{3.1}$$

where A represents the amplitude, μ the temporal offset (mean), and σ the standard deviation controlling the width of the function.

In our hybrid model, each cardiac electrical event within a single heartbeat is represented by one or more Gaussian components, positioned relative to the R-peak time t_R:

- **P wave**: Modeled as a single Gaussian representing atrial depolarization
- **QRS complex**: Represented by three Gaussians (Q, R, S waves) capturing ventricular depolarization
- **ST segment**: Modeled as a wide, low-amplitude Gaussian representing early repolarization
- **T wave**: Composed of two Gaussians allowing for asymmetric morphology

The complete single-beat waveform is constructed as:

$$W(t) = G_P(t) + G_{QRS}(t) + G_{ST}(t) + G_T(t) \tag{3.2}$$

where each component is defined relative to the R-peak:

$$G_P(t) = G(t, A_P, t_R + \mu_P, \sigma_P) \tag{3.3}$$

$$G_{QRS}(t) = \sum_{i \in \{Q,R,S\}} G(t, A_i, t_R + \mu_i, \sigma_i) \tag{3.4}$$

$$G_{ST}(t) = G(t, A_{ST}, t_R + \mu_{ST}, \sigma_{ST}) \tag{3.5}$$

$$G_T(t) = G(t, A_{T1}, t_R + \mu_{T1}, \sigma_{T1}) + G(t, A_{T2}, t_R + \mu_{T2}, \sigma_{T2}) \tag{3.6}$$

3.2.2 Dipole Model and Spatial Projection

The heart's electrical activity can be approximated as an equivalent current dipole vector $\mathbf{d}(t) = [d_x(t), d_y(t), d_z(t)]$ located at the heart's electrical center [51]. This representation, while simplified, captures the essential spatial characteristics of cardiac electrical propagation and has been fundamental to understanding ECG lead systems since the work of Frank [47] and Wilson [53].

The dipole components are constructed as weighted combinations of the Gaussian waveform components:

$$d_x(t) = w_{Px}G_P(t) + w_{QRSx}G_{QRS}(t) + w_{STx}G_{ST}(t) + w_{Tx}G_T(t) \tag{3.7}$$

$$d_y(t) = w_{Py}G_P(t) + w_{QRSy}G_{QRS}(t) + w_{STy}G_{ST}(t) + w_{Ty}G_T(t) \tag{3.8}$$

$$d_z(t) = w_{Pz}G_P(t) + w_{QRSz}G_{QRS}(t) + w_{STz}G_{ST}(t) + w_{Tz}G_T(t) \tag{3.9}$$

The weights w_{ij} reflect the relative contribution of each cardiac event to the overall dipole moment in each spatial direction, derived from physiological understanding and empirical observations [5].

The potential measured by any ECG lead is obtained through vector projection:

$$V_{lead}(t) = \mathbf{d}(t) \cdot \mathbf{L}_{lead} = d_x(t)L_x + d_y(t)L_y + d_z(t)L_z \tag{3.10}$$

where $\mathbf{L}_{lead} = [L_x, L_y, L_z]$ represents the lead vector for the specific ECG lead.

For the standard 12-lead system, the lead vectors are defined according to conventional electrode placements [4]. The limb leads follow the Einthoven triangle configuration, while precordial leads capture the heart's electrical activity from the horizontal plane.

3.3 Methodology

3.3.1 Data Source and Preprocessing

Our parameter estimation utilizes the MIT-BIH Arrhythmia Database [52], a gold standard resource containing 48 half-hour ambulatory ECG recordings sampled at 360 Hz. The database provides both raw signal data and expert annotations for R-peak locations and arrhythmia classifications, making it an invaluable resource for cardiovascular research [14].

The preprocessing pipeline involves several key steps:

1. **Data loading**: ECG records are accessed using the WFDB Python package [15], with automatic download if not locally available
2. **Signal segmentation**: Representative segments containing multiple cardiac cycles are extracted based on R-peak annotations
3. **Signal conditioning**: Basic filtering and noise reduction are applied to improve feature detection accuracy [21]

For this study, we primarily focus on Lead II recordings, as this lead provides excellent visualization of atrial and ventricular activity and is commonly used for rhythm analysis [1].

3.3.2 Parameter Extraction

Accurate parameter estimation forms the foundation of realistic ECG simulation. We employ the NeuroKit2 library [54], a comprehensive physiological signal processing package, for automated feature extraction.

The parameter extraction process includes:

1. **R-peak refinement**: While R-peaks are available from MIT-BIH annotations, we apply additional peak detection algorithms to ensure consistency [39]
2. **Wave delineation**: P and T wave peaks are identified using discrete wavelet transform methods [22]
3. **Statistical analysis**: Mean values and variability measures are computed for key parameters including wave amplitudes, temporal offsets, and durations

Key extracted parameters include:

- P wave offset (μ_P): Average time difference between P-peaks and corresponding R-peaks
- T wave offset (μ_T): Average time difference between T-peaks and corresponding R-peaks
- Wave amplitudes (A_P, A_R, A_T): Mean signal amplitudes at respective peak locations
- Heart rate variability measures for rhythm generation [55]

3.3.3 Lead II Simulation Implementation

The Lead II simulation focuses on generating a single-lead ECG signal using extracted parameters from real data. The implementation follows these steps:

1. **Parameter initialization**: Gaussian parameters are set based on extracted statistics, with physiologically reasonable defaults for undetected features
2. **Waveform generation**: For each cardiac cycle, individual Gaussian components are generated and combined
3. **Dipole calculation**: The 3D dipole vector is computed using predefined weights
4. **Lead projection**: The dipole is projected onto the Lead II vector to obtain the final signal
5. **Noise addition**: Realistic noise components including baseline wander and high-frequency artifacts are incorporated [56]
6. **Signal scaling**: The synthetic signal is scaled to match the statistical properties of the reference signal

This detailed process allows the Lead II code script to generate a synthetic Lead II ECG signal that is morphologically similar to a target real ECG segment, based on extracted parameters and the hybrid Gaussian-Dipole model. The workflow of the Lead II script is illustrated in Figure 3.1.

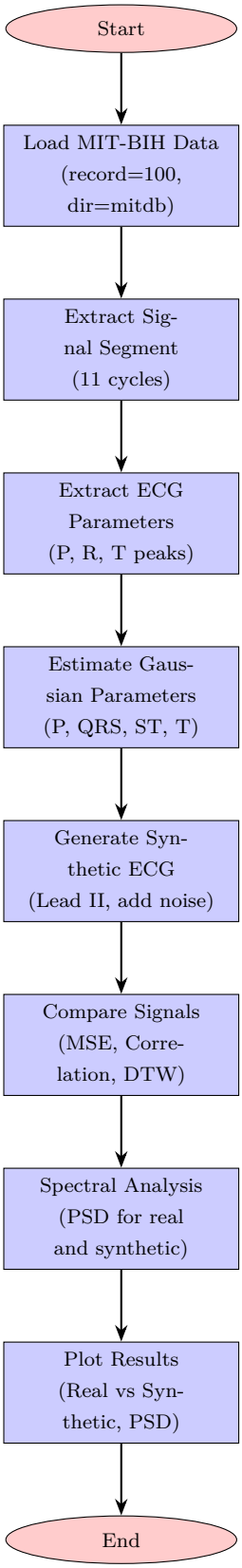

Figure 3.1: Lead II code flowchart

3.3.4 12-Lead ECG Simulation

The 12-lead simulation extends the single-lead approach to generate a complete standard ECG. Key enhancements include:

1. **Multi-lead projection**: The same dipole vector is projected onto all 12 standard lead vectors simultaneously
2. **Pathology simulation**: Specific parameter modifications simulate common cardiac abnormalities
3. **Independent noise**: Each lead receives independent noise components to simulate realistic recording conditions

3.3.4.1 Pathological Condition Simulation

The model's flexibility allows simulation of various cardiac abnormalities through targeted parameter modifications:

- **Ischemia**: ST segment elevation and T wave inversion through amplitude adjustments
- **Atrial fibrillation**: P wave suppression and irregular R-R intervals
- **Ventricular tachycardia**: Increased heart rate and widened QRS complexes
- **Bradycardia**: Reduced heart rate with normal morphology

These pathological patterns are based on established clinical criteria and electrophysiological understanding [57, 1].

The workflow of the 12 leads script, including pathology simulation, is illustrated in Figure 3.2.

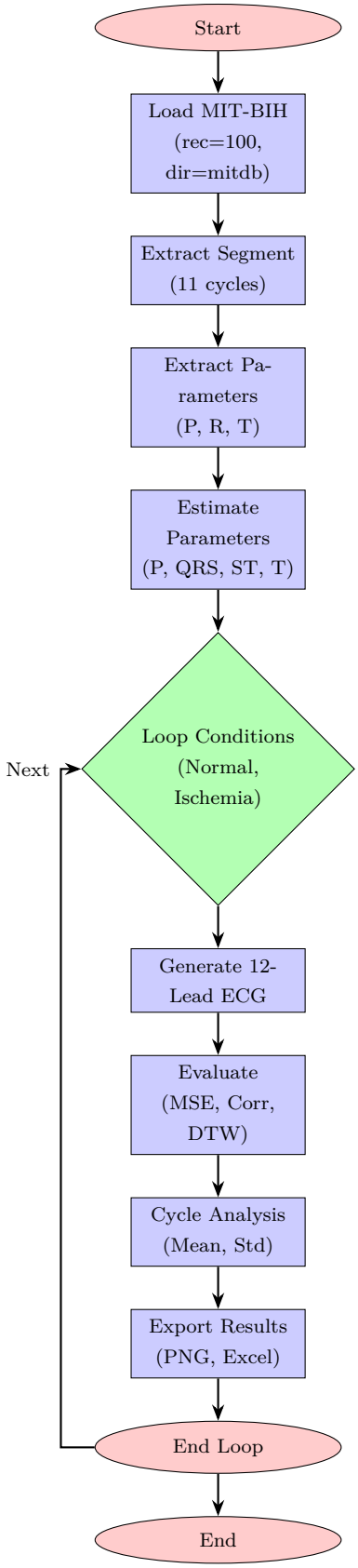

Figure 3.2: 12-Lead code flowchart

3.4 Results and Evaluation

3.4.1 Lead II Simulation Performance

The Lead II simulation was evaluated using MIT-BIH record 100, demonstrating strong quantitative performance:

- Mean Squared Error: 0.0065
- Correlation Coefficient: 0.8859
- Dynamic Time Warping Distance: 2.2441
- Match Percentage: 88.59%

These metrics indicate excellent morphological similarity between synthetic and real signals. The high correlation coefficient suggests the model successfully captures the overall waveform characteristics, while the low MSE indicates minimal amplitude differences.

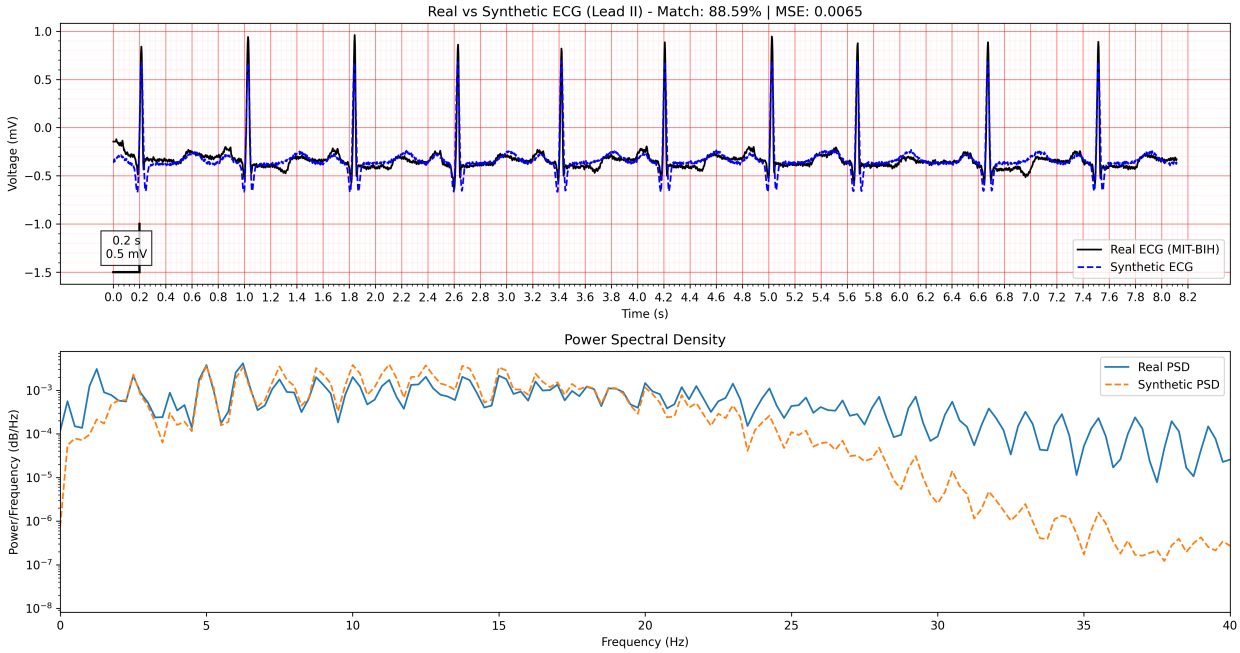

Figure 3.3: Comparison of Real (MIT-BIH Record 100, Lead II segment) and Synthetic Lead II ECG signals generated by Lead II code. (Top) Time-domain signals. (Bottom) Power Spectral Densities (PSDs). Quantitative metrics (MSE, Correlation, Match %) are displayed.

3.4.2 12-Lead Simulation Results

The 12-lead simulations produced visually recognizable ECG patterns for both normal and pathological conditions. Performance metrics for various simulated conditions are summarized in Table 3.1.

Table 3.1: Performance metrics for 12-lead ECG simulations

Condition	**MSE**	**Correlation**	**DTW**	**PSD Corr.**	**Match (%)**
Normal	0.0687	0.7640	5.4638	0.7139	76.40
Ischemia	0.0802	0.7843	6.0522	0.7674	78.43
Atrial Fibrillation	0.0837	0.7374	6.7937	0.6899	73.74
Ventricular Tachycardia	0.1088	0.8197	7.8972	0.7917	81.97
Bradycardia	0.0671	0.7547	5.3517	0.6865	75.47

The results demonstrate the model's capability to generate distinguishable patterns for different pathological conditions while maintaining reasonable similarity to expected morphologies. This is evident through qualitative assessment of the generated pathological ECGs (visualized in Figures 3.5a to 3.5d), which demonstrates the following key findings:

- **Ischemia (Fig. 3.5a):** The simulation exhibit ST-segment elevation and potentially T-wave inversion in specific leads, consistent with the parameter modifications (A_{ST} increase, A_{T2} inversion). The location of these changes (which leads are affected) depended on the underlying dipole modification but is generalized in this simulation.
- **Atrial Fibrillation (Fig. 3.5b):** The simulation showed an irregularly irregular rhythm (varying R-R intervals) and absent or replaced P waves (often by fibrillatory waves, though the model simplifies this by setting $A_P = 0$).
- **Ventricular Tachycardia (Fig. 3.5c):** The simulation displayed a rapid heart rate and wide QRS complexes, consistent with the increased rate and widened Gaussian parameters ($\sigma_Q, \sigma_R, \sigma_S$). P waves were dissociated or absent.
- **Bradycardia (Fig. 3.5d):** The simulation showed a slow, regular rhythm with normal P-QRS-T morphology, reflecting the decreased heart rate parameter.

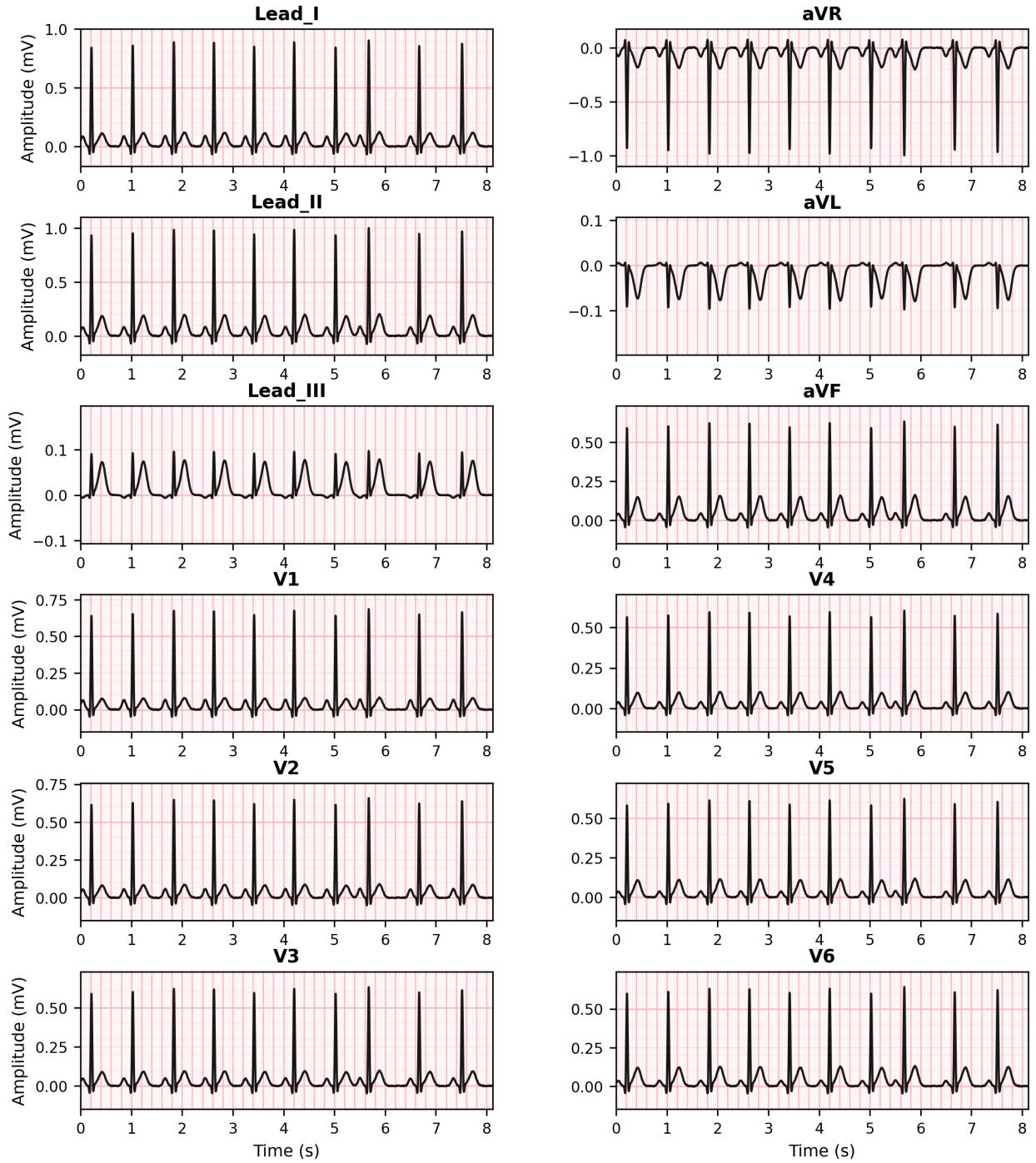

Figure 3.4: Simulated Normal Sinus Rhythm 12-Lead ECG generated by 12 Leads Code (Calibration: 25 mm/s paper speed, 10 mm/mV sensitivity)

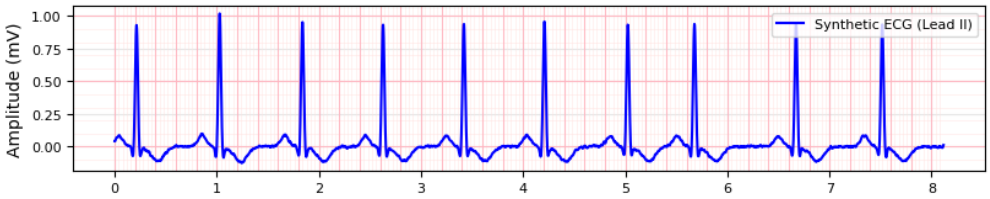

(a) Ischemia

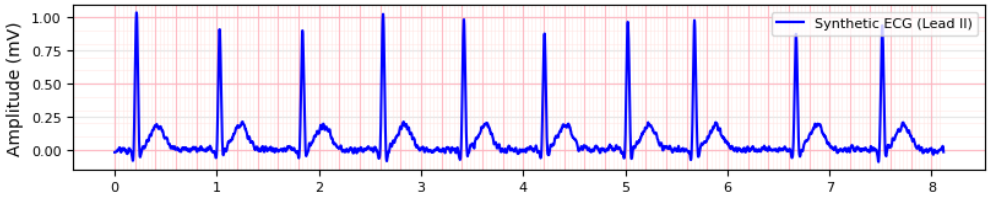

(b) Atrial Fibrillation

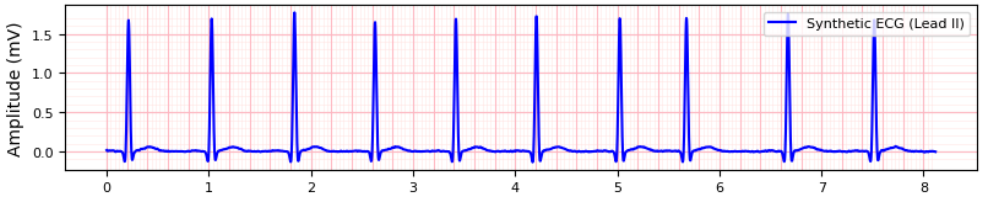

(c) Ventricular Tachycardia

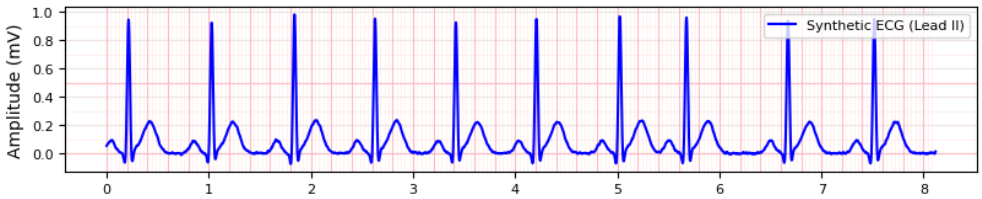

(d) Bradycardia

Figure 3.5: Synthetic Lead II ECGs simulating various pathological conditions generated by 12 Leads Code (Calibration: 25 mm/s paper speed, 10 mm/mV sensitivity).

3.4.3 Spectral Analysis

Power spectral density analysis revealed good frequency domain matching between synthetic and reference signals. The PSD correlation values ranged from 0.69 to 0.79 across different conditions, indicating that the model captures not only time-domain morphology but also essential frequency characteristics [58].

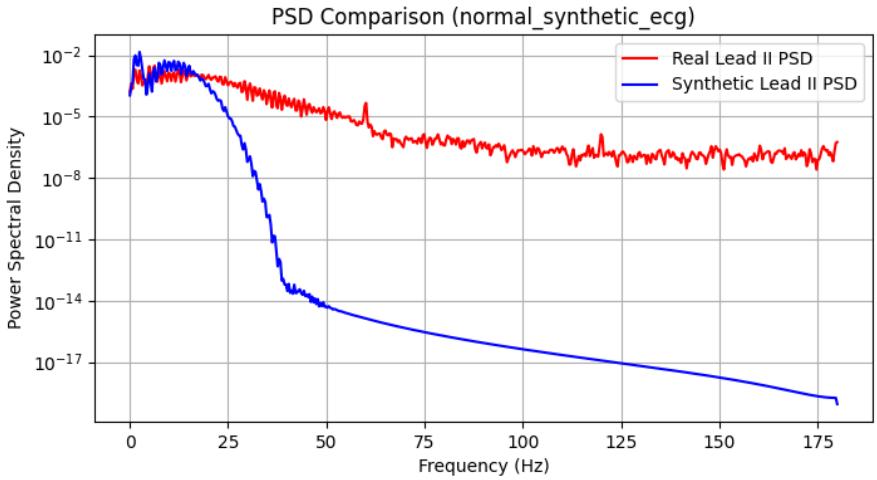

Figure 3.6: Power Spectral Density (PSD) analysis for the synthetic Normal Sinus Rhythm 12-Lead ECG.

3.5 Discussion

3.5.1 Model Strengths

The hybrid Gaussian-Dipole approach offers several significant advantages:

1. **Computational efficiency**: The model generates ECG signals rapidly, making it suitable for large-scale studies and real-time applications
2. **Physiological interpretation**: Parameters have clear relationships to cardiac electrophysiology, facilitating intuitive control and modification [59]
3. **Flexibility**: The framework easily accommodates simulation of various pathological conditions through targeted parameter adjustments
4. **Multi-lead capability**: Single parameter sets generate consistent 12-lead ECGs through spatial projection

3.5.2 Current Limitations

Several limitations must be acknowledged:

1. **Simplified cardiac representation**: The single dipole model cannot capture all complexities of distributed cardiac electrical activity [60]
2. **Fixed Gaussian shapes**: Real ECG morphology exhibits greater variability than fixed Gaussian functions can represent
3. **Approximate lead vectors**: The model uses simplified lead vectors that may not account for individual anatomical variations
4. **Limited beat-to-beat variability**: Normal physiological variations in rhythm and morphology are not fully captured [61]

3.5.3 Validation and Clinical Relevance

The quantitative metrics demonstrate the model's ability to generate ECG signals with strong similarity to real recordings. The correlation coefficients above 0.76 for all conditions indicate good morphological fidelity. However, comprehensive validation requires testing across diverse patient populations and pathological conditions.

The model's educational value is particularly noteworthy. The ability to generate controlled, labeled ECG patterns makes it valuable for training automated analysis algorithms and educating healthcare professionals. The pathology simulation capabilities enable creation of rare or complex scenarios that might be difficult to obtain from clinical databases.

3.6 Future Directions

3.6.1 Model Enhancements

Several avenues for improvement merit investigation:

1. **Advanced parameter estimation**: Machine learning approaches could optimize parameter extraction from multi-lead recordings [10]
2. **Multi-dipole models**: Incorporating multiple dipoles could better represent complex cardiac electrical patterns

3. **Patient-specific modeling**: Integration with medical imaging could enable personalized lead vector calculations [62]

4. **Enhanced variability**: Incorporation of physiological variability models would improve realism [63]

3.6.2 Extended Applications

The framework's flexibility suggests several promising applications:

1. **Algorithm development**: Providing diverse training data for machine learning-based ECG analysis systems [64]

2. **Device testing**: Supporting development and validation of ECG monitoring devices [23]

3. **Clinical decision support**: Generating reference patterns for automated diagnostic systems

4. **Research tools**: Enabling controlled studies of ECG interpretation and analysis methods

3.6.3 Integration with Advanced Models

Future work could explore integration with more sophisticated cardiac models:

1. **Electrophysiological coupling**: Linking Gaussian parameters to cellular-level electrical activity [65, 66]

2. **Anatomical integration**: Incorporating realistic heart geometry and tissue properties [67]

3. **Hemodynamic interactions**: Modeling the relationship between electrical activity and mechanical function [68]

3.7 Conclusions

This study successfully demonstrates the application of a hybrid Gaussian-Dipole model for ECG simulation, achieving a practical balance between computational efficiency and physiological realism. The model's ability to generate both single-lead and 12-lead ECG signals

with good fidelity to real recordings, combined with its flexibility in simulating pathological conditions, establishes its value for research, education, and algorithm development.

The quantitative evaluation revealed strong performance, with correlation coefficients exceeding 0.76 for all tested conditions and achieving 0.89 for the carefully parameterized Lead II simulation. The model's capability to simulate common cardiac abnormalities through intuitive parameter modifications demonstrates its practical utility for diverse applications [69].

While current limitations existparticularly regarding the simplified cardiac representation and fixed morphological constraintsthe framework provides a solid foundation for future enhancements. The computational efficiency and physiological interpretability make it particularly suitable for educational applications and algorithm testing scenarios where large volumes of controlled, labeled data are required.

Looking forward, this work establishes a foundation for more sophisticated hybrid modeling approaches that could incorporate patient-specific anatomical information, advanced physiological variability, and integration with detailed electrophysiological models. Such developments would further enhance the model's clinical relevance while maintaining its computational advantages.

The hybrid Gaussian-Dipole approach represents a valuable contribution to the toolkit of ECG simulation methods, offering researchers and educators a practical, flexible, and physiologically meaningful framework for generating synthetic cardiac electrical signals. As computational modeling continues to play an increasingly important role in cardiovascular medicine [70], such tools will prove essential for advancing our understanding of cardiac electrophysiology and improving diagnostic capabilities.

General conclusion

This thesis has successfully developed and evaluated a hybrid Gaussian-Dipole model for ECG simulation, offering a practical solution for generating realistic ECG signals. By integrating Gaussian functions to model the P, QRS, ST, and T waves with a dipole-based representation of the hearts electrical activity, the model achieves a balance between computational efficiency and physiological plausibility.

Using the MIT-BIH Arrhythmia Database, the model was parameterized to simulate Lead II and 12-lead ECGs, demonstrating high fidelity for Lead II (correlation of 0.89, MSE of 0.0065) and reasonable performance across 12 leads, with effective simulation of pathologies like ischemia and ventricular tachycardia. These results were validated using metrics such as Mean Squared Error, Correlation, Dynamic Time Warping Distance, and Power Spectral Density Correlation, confirming the models ability to capture key morphological and frequency characteristics.

The hybrid models strengths lie in its efficiency, flexibility, and applicability to algorithm validation, medical education, and cardiac research. Compared to computationally intensive biophysical models, it offers a faster alternative suitable for real-time applications. Its adjustable parameters enable simulation of various cardiac conditions, making it a valuable tool for training and testing. However, limitations include less accurate 12-lead parameter estimation, simplified dipole assumptions, and limited capture of beat-to-beat variability. These challenges highlight opportunities for future work, such as automated parameter extraction, multi-dipole models, patient-specific lead vectors, and enhanced variability and noise models.

The contributions of this thesis extend beyond the model itself, providing a framework for integrating theoretical insights from cardiac electrophysiology with practical simulation techniques. The model supports advancements in diagnostic algorithm development, medical training simulators, and computational cardiology, with potential to improve patient outcomes through enhanced diagnostic tools. Moving forward, refining the models physiological accuracy and expanding its scope to include a broader range of pathologies will further strengthen its impact.

This work underscores the power of interdisciplinary approaches in medical physics, bridging theoretical foundations with practical applications to advance our understanding and management of cardiac health.

Bibliography

[1] Galen S. Wagner and David G. Strauss. *Marriott's Practical Electrocardiography*. Lippincott Williams & Wilkins, 2014.

[2] A. D. Waller. A demonstration of man's electrical field of force. *The Journal of Physiology*, 8(5–6):229–234, 1887.

[3] Willem Einthoven. Eine neue empfangsapparatur für die galvanischen schwankungen des menschlichen herzmuskels und die ergebnisse ihrer anwendung bei der untersuchung des regelmäSSigen herzschlags. *Archiv für die gesamte Physiologie des Menschen und der Tiere*, 99(5):415–434, 1903.

[4] Paul Kligfield, Leonard S. Gettes, James J. Bailey, Rory Childers, Barbara J. Deal, E. William Hancock, Gerard van Herpen, Jan A. Kors, Peter Macfarlane, David M. Mirvis, Olle Pahlm, Pentti Rautaharju, and Galen S. Wagner. Recommendations for the standardization and interpretation of the electrocardiogram: Part i: The electrocardiogram and its technology. *Circulation*, 115(10):1306–1324, 2007.

[5] Jaakko Malmivuo and Robert Plonsey. *Bioelectromagnetism: Principles and Applications of Bioelectric and Biomagnetic Fields*. Oxford University Press, USA, 1995.

[6] Peter W. Macfarlane, Adriaan Van Oosterom, Olle Pahlm, Paul Kligfield, Michiel Janse, and John Camm. *Comprehensive Electrocardiology*. Springer, 2010.

[7] Piero Colli Franzone, Luca Franco Pavarino, and Simone Scacchi. *Mathematical Cardiac Electrophysiology*, volume 13. Springer, 2014.

[8] Robert Plonsey and Roger C. Barr. *Bioelectricity: A Quantitative Approach*. Springer, 3 edition, 2007.

[9] R. H. Clayton, O. Bernus, E. M. Cherry, H. Dierckx, F. H. Fenton, L. Mirabella, A. V. Panfilov, F. B. Sachse, G. Seemann, and P. Taggart. Models of cardiac tissue elec-

trophysiology: Progress, challenges and open questions. *Progress in Biophysics and Molecular Biology*, 104(1–3):22–48, 2011.

[10] Pranav Rajpurkar, Awni Y. Hannun, Masoumeh Haghpanahi, Codie Bourn, and Andrew Y. Ng. Cardiologist-level arrhythmia detection with convolutional neural networks. *arXiv preprint arXiv:1707.01836*, 2017.

[11] Miguel A. Quiroz-Juárez, Orlando R. Jiménez-Ramírez, Rubén Vázquez-Medina, Elena Ryzhii, Maxim Ryzhii, Arturo García-García, Mario Pérez-Meza, Pedro Cortés-Antonio, and Gerardo Sánchez-Ortiz. Ecg patient simulator based on mathematical models. *Sensors*, 22(15):5786, 2022.

[12] Ramesh M. Gulrajani. The forward and inverse problems of electrocardiography. *IEEE Engineering in Medicine and Biology Magazine*, 17(5):84–101, 1998.

[13] Andrew Pullan, Leo Cheng, Martyn Nash, Alireza Ghodrati, Rob Macleod, and Dana Brooks. The inverse problem of electrocardiography. 2010.

[14] Ary L. Goldberger, Luis A. N. Amaral, Leon Glass, Jeffrey M. Hausdorff, Plamen Ch. Ivanov, Roger G. Mark, Joseph E. Mietus, George B. Moody, Chung-Kang Peng, and H. Eugene Stanley. Physiobank, physiotoolkit, and physionet: Components of a new research resource for complex physiologic signals. *Circulation*, 101(23):e215–e220, 2000.

[15] PhysioNet. Wfdb-python: A python package for reading and writing physiological signals. https://github.com/MIT-LCP/wfdb-python, 2021.

[16] Gari D. Clifford, Chengyu Liu, Benjamin Moody, Li-wei H. Lehman, Ikaro Silva, Qiao Li, Alistair E. W. Johnson, and Roger G. Mark. Af classification from a short single lead ecg recording: The physionet/computing in cardiology challenge 2017. In *Computing in Cardiology*, volume 44, pages 1–4. IEEE, 2017.

[17] Patrick E. McSharry, Gari D. Clifford, Lionel Tarassenko, and Leonard A. Smith. A dynamical model for generating synthetic electrocardiogram signals. *IEEE Transactions on Biomedical Engineering*, 50(3):289–294, 2003.

[18] Chinyere Elendu, Daniel C. Amaechi, Amara U. Okatta, Evangeline C. Amaechi, Tochi C. Elendu, Chukwuemeka P. Ezeh, and Ijeoma D. Elendu. The impact of simulation-based training in medical education: A review. *Medicine*, 103(27):e38813, 2024.

[19] Marco Piccolino. Animal electricity and the birth of electrophysiology: the legacy of luigi galvani. *Brain Research Bulletin*, 46(5):381–407, 1998.

[20] Thomas Lewis. *The Mechanism and Graphic Registration of the Heart Beat*. Shaw and Sons, London, 1920.

[21] Leif Sörnmo and Pablo Laguna. *Bioelectrical Signal Processing in Cardiac and Neurological Applications*. Elsevier, 2005.

[22] Radek Martinek, Martina Ladrova, Michaela Sidikova, Rene Jaros, Khosrow Behbehani, Radana Kahankova, and Aleksandra Kawala-Sterniuk. Advanced bioelectrical signal processing methods: Past, present and future approachpart i: Cardiac signals. *Sensors*, 21(15):5186, 2021.

[23] Zeineb Bouzid, Salah S. Al-Zaiti, Raymond Bond, and Ervin Sejdi. Remote and wearable ecg devices with diagnostic abilities in adults: A state-of-the-science scoping review. *Heart Rhythm*, 19(7):1192–1201, 2022.

[24] Shu-Li Guo, Li-Na Han, Hong-Wei Liu, Quan-Jin Si, De-Feng Kong, and Fu-Su Guo. The future of remote ecg monitoring systems. *Journal of Geriatric Cardiology*, 13(6):528, 2016.

[25] Sudha Ramasamy and Archana Balan. Wearable sensors for ecg measurement: A review. *Sensor Review*, 38(4):412–419, 2018.

[26] Keith L. Moore and Arthur F. Dalley. *Clinically Oriented Anatomy*. Wolters Kluwer India Pvt Ltd, 2018.

[27] Susan Standring, Harold Ellis, and Caroline Wigley. *Gray's Anatomy: The Anatomical Basis of Clinical Practice*. Elsevier Churchill Livingstone, 39 edition, 2005.

[28] Robert H. Anderson, Edward J. Baker, Andrew Redington, Michael L. Rigby, Daniel Penny, and Gil Wernovsky. *Paediatric Cardiology*. Elsevier Health Sciences, 2009.

[29] Horia Muresian. The clinical anatomy of the right ventricle. *Clinical Anatomy*, 29(3):380–398, 2016.

[30] Valve human. Wikimedia Commons, 2023.

[31] Abdellaziz Dahou, Dmitry Levin, Mark Reisman, and Rebecca T. Hahn. Anatomy and physiology of the tricuspid valve. *JACC: Cardiovascular Imaging*, 12(3):458–468, 2019.

[32] Robert B. Hinton and Katherine E. Yutzey. Heart valve structure and function in development and disease. *Annual Review of Physiology*, 73(1):29–46, 2011.

[33] Ralph Shabetai. *The Pericardium*, volume 249. Springer Science & Business Media, 2003.

[34] Richard Gordan, Judith K. Gwathmey, and Lai-Hua Xie. Autonomic and endocrine control of cardiovascular function. *World Journal of Cardiology*, 7(4):204, 2015.

[35] Thomas N. James. The internodal pathways of the human heart. *Progress in Cardiovascular Diseases*, 43(6):495–535, 2001.

[36] Roshan Karki, Anvi Raina, Fatima M. Ezzeddine, Melanie C. Bois, and Samuel J. Asirvatham. Anatomy and pathology of the cardiac conduction system. *Cardiac Electrophysiology Clinics*, 13(4):569–584, 2021.

[37] Yasar Sattar and Lovely Chhabra. Electrocardiogram. In *StatPearls*. StatPearls Publishing, 2023.

[38] William F. Ganong. *Review of Medical Physiology*. Prentice-Hall International, 17 edition, 1995.

[39] Gari D. Clifford, Francisco Azuaje, and Patrick E. McSharry. *Advanced Methods and Tools for ECG Data Analysis*. Artech House, 2006.

[40] Adam Paine, Akash Premkumar, and Thoralf M. Sundt. *Pericardial Disease*, pages 289–297. Springer International Publishing, Cham, 2024.

[41] Beatrice Zanchi, Giuliana Monachino, Luigi Fiorillo, Giulio Conte, Angelo Auricchio, Athina Tzovara, and Francesca D. Faraci. Synthetic ecg signals generation: A scoping review. *Computers in Biology and Medicine*, 184:109453, 2025.

[42] A. van Oosterom. The forward problem of electrocardiography. In *Comprehensive Electrocardiology*, pages 291–306. Springer, 1998.

[43] Alan L. Hodgkin and Andrew F. Huxley. A quantitative description of membrane current and its application to conduction and excitation in nerve. *The Journal of Physiology*, 117(4):500–544, 1952.

[44] Richard FitzHugh. Impulses and physiological states in theoretical models of nerve membrane. *Biophysical Journal*, 1(6):445–466, 1961.

[45] Craig S. Henriquez. Simulating the electrical behavior of cardiac tissue using the bidomain model. *Critical Reviews in Biomedical Engineering*, 21(1):1–77, 1993.

[46] S. R. F. S. M. Gois and M. A. Savi. An analysis of heart rhythm dynamics using a three-coupled oscillator model. *Chaos, Solitons & Fractals*, 41(5):2553–2565, 2009.

[47] Ernest Frank. An accurate, clinically practical system for spatial vectorcardiography. *Circulation*, 13(5):737–749, 1956.

[48] Willem Einthoven, George Fahr, and A. De Waart. On the direction and manifest size of the variations of potential in the human heart and on the influence of the position of the heart on the form of the electrocardiogram. *American Heart Journal*, 40(2):163–211, 1950.

[49] Reza Sameni, Gari D Clifford, Christian Jutten, and Mohammad B Shamsollahi. Multichannel ecg and noise modeling: Application to maternal and fetal ecg signals. *EURASIP Journal on Advances in Signal Processing*, 2007:1–14, 2007.

[50] Mark Potse, Bruno Dubé, Jacques Richer, Alain Vinet, and Ramesh M. Gulrajani. A comparison of monodomain and bidomain reaction-diffusion models for action potential propagation in the human heart. *IEEE Transactions on Biomedical Engineering*, 53(12):2425–2435, 2006.

[51] David B. Geselowitz. Dipole theory in electrocardiography. *The American Journal of Cardiology*, 14(3):301–306, 1964.

[52] George B. Moody and Roger G. Mark. The impact of the mit-bih arrhythmia database. *IEEE Engineering in Medicine and Biology Magazine*, 20(3):45–50, 2001.

[53] Frank N. Wilson, Franklin D. Johnston, Angus G. Macleod, and Paul S. Barker. Electrocardiograms that represent the potential variations of a single electrode. *American Heart Journal*, 23(4):447–458, 1944.

[54] Dominique Makowski, Tam Pham, Zen J. Lau, Jan C. Brammer, François Lespinasse, Hung Pham, Christopher Schölzel, and S. H. Annabel Chen. Neurokit2: A python toolbox for neurophysiological signal processing. *Behavior Research Methods*, 53(4):1689–1696, 2021.

[55] Marek Malik and A. John Camm. *Heart Rate Variability*. Futura Publishing Company, 1995.

[56] Pablo Laguna, George B. Moody, and Roger G. Mark. Power spectral density of unevenly sampled data by least-square analysis: Performance and application to heart rate signals. *IEEE Transactions on Biomedical Engineering*, 45(6):698–715, 1998.

[57] Borys Surawicz and Timothy K. Knilans. *Chou's Electrocardiography in Clinical Practice*. Saunders, 6 edition, 2008.

[58] Ronald D. Berger, Solange Akselrod, David Gordon, and Richard J. Cohen. An efficient algorithm for spectral analysis of heart rate variability. *IEEE Transactions on Biomedical Engineering*, 33(9):900–904, 1986.

[59] Denis Noble. Modeling the heart–from genes to cells to the whole organ. *Science*, 295(5560):1678–1682, 2002.

[60] Andre G. Kleber and Yoram Rudy. Basic mechanisms of cardiac impulse propagation and associated arrhythmias. *Physiological Reviews*, 84(2):431–488, 2004.

[61] Task Force of the European Society of Cardiology. Heart rate variability: Standards of measurement, physiological interpretation, and clinical use. *Circulation*, 93(5):1043–1065, 1996.

[62] Fijoy Vadakkumpadan, Hermenegild Arevalo, Anton J. Prassl, Jianghong Chen, Florian Kickinger, Peter Kohl, Gernot Plank, and Natalia A. Trayanova. Image-based models of cardiac structure in health and disease. *Wiley Interdisciplinary Reviews: Systems Biology and Medicine*, 2(4):489–506, 2010.

[63] Adityo Prakosa, Hermenegild J. Arevalo, Dongdong Deng, Patrick M. Boyle, Plamen P. Nikolov, Hiroshi Ashikaga, Joshua J. E. Blauer, Sohail Zahid, Benjamin D. Atwater, Esther W. Remme, et al. Personalized virtual-heart technology for guiding the ablation of infarct-related ventricular tachycardia. *Nature Biomedical Engineering*, 2(10):732–740, 2018.

[64] Ian Goodfellow, Jean Pouget-Abadie, Mehdi Mirza, Bing Xu, David Warde-Farley, Sherjil Ozair, Aaron Courville, and Yoshua Bengio. Generative adversarial nets. In *Advances in Neural Information Processing Systems*, volume 27, 2014.

[65] Chun-Hua Luo and Yoram Rudy. A model of the ventricular cardiac action potential. *Circulation Research*, 68(6):1501–1526, 1991.

[66] Denis Noble. A modification of the hodgkin–huxley equations applicable to purkinje fibre action and pacemaker potentials. *The Journal of Physiology*, 160(2):317–352, 1962.

[67] Peter J. Hunter and Thomas K. Borg. Integration from proteins to organs: The physiome project. *Nature Reviews Molecular Cell Biology*, 4(3):237–243, 2003.

[68] Arthur C. Guyton and John E. Hall. *Textbook of Medical Physiology*. Elsevier, 14 edition, 2021.

[69] Katelyn Gillette, Christoph M. Augustin, Maxime Defauw, Nele Vandersickel, et al. Medalcare-xl: 16900 healthy and pathological synthetic 12-lead ecgs generated using a mechanistic cardiac electrophysiology model. *Scientific Data*, 10(1):453, 2023.

[70] Catherine H. Crouch and Eitan Fattal. Teaching the electrical origins of the electrocardiogram. *American Journal of Physics*, 88(7):526–534, 2020.

[71] Jinichi Nagumo, Suguru Arimoto, and Shuji Yoshizawa. An active pulse transmission line simulating nerve axon. *Proceedings of the IRE*, 50(10):2061–2070, 1962.

[72] Leslie Tung. *A Bi-domain Model for Describing Ischemic Myocardial DC Potentials*. PhD thesis, MIT, 1978.

[73] Galen S. Wagner. *Marriott's Practical Electrocardiography*. Lippincott Williams & Wilkins, 11 edition, 2008.

[74] Diederik P. Kingma and Max Welling. Auto-encoding variational bayes. *arXiv preprint arXiv:1312.6114*, 2013.

[75] James Keener and James Sneyd. *Mathematical Physiology: I: Cellular Physiology*. Springer, 2009.

[76] Joseph J. Maleszewski, Chi K. Lai, Vidhya Nair, and John P. Veinot. Anatomic considerations and examination of cardiovascular specimens (excluding devices). *Cardiovascular Pathology*, pages 27–84, 2022.

[77] Michael G. Bateman, Jason L. Quill, Alexander J. Hill, and Paul A. Iaizzo. The anatomy and function of the semilunar valves. In *Heart Valves: From Design to Clinical Implantation*, pages 27–43. Springer, 2023.

[78] E. Rene Rodriguez and Carmela D. Tan. Structure and anatomy of the human pericardium. *Progress in Cardiovascular Diseases*, 59(4):327–340, 2017.

[79] Hui Yuan and Wenguo Cui. The lubricated matter in body. *Progress in Materials Science*, page 101334, 2024.

[80] Portonovo S. Ayyaswamy. Introduction to biofluid mechanics. *Fluid Mechanics*, 6:e1–e73, 2016.

[81] Physiopedia. Anatomy of the human heart, 2024. [Online; accessed 16-May-2025].

[82] A. Boardman, Fernando S. Schlindwein, Ana Paula Rocha, and A. Leite. A study on the optimum order of autoregressive models for heart rate variability. *Physiological Measurement*, 23(2):325, 2002.

[83] Gordon E. Dower, Helio B. Machado, and John A. Osborne. On deriving the electrocardiogram from vectorcardiographic leads. *Clinical Cardiology*, 3(2):87–95, 1980.

[84] Tatsuo Togawa, P. Ake Oberg, and Francis A. Spelman. *Biomedical Transducers and Instruments*. CRC Press, 1997.

[85] Janice M. Jenkins and Susan A. Caswell. Detection algorithms in implantable cardioverter defibrillators. *Proceedings of the IEEE*, 84(3):428–445, 1998.

[86] Augustus O. Grant. Cardiac ion channels. *Circulation: Arrhythmia and Electrophysiology*, 2(2):185–194, 2009.

[87] Arnold M. Katz. *Physiology of the Heart*. Lippincott Williams & Wilkins, 2010.

[88] Karri Haen Whitmer. A mixed course-based research approach to human physiology. 2021.